Cellular Signalling 97 (2022) 110386

Contents lists available at ScienceDirect

Cellular Signalling

journal homepage: www.elsevier.com/locate/cellsig

Glutamatergic transmission and receptor expression in the synucleinopathy h-α-synL62 mouse model: Effects of hydromethylthionine

Karima Schwab [a,b,*], Zoi Chasapopoulou [b,c], Silke Frahm [b,d], Mandy Magbagbeolu [b], Anna Cranston [a,e], Charles R. Harrington [a,f], Claude M. Wischik [a,f], Franz Theuring [b], Gernot Riedel [a,*]

[a] School of Medicine, Medical Sciences and Nutrition, University of Aberdeen, Foresterhill, Aberdeen AB25 2ZD, UK
[b] Institute of Pharmacology, Charité - Universitätsmedizin Berlin, Hessische Str. 3-4, 10115 Berlin, Germany
[c] Center for Stroke Research, Department of Experimental Neurology, Charité - Universitätsmedizin Berlin, Robert Koch Platz 4, 101155 Berlin, Germany
[d] Stem Cell Core Facility, Max-Delbrück-Centrum für Molekulare Medizin, Robert-Rössle-Straße 10, 13125 Berlin, Germany
[e] Benchsci, Montreal, Quebec, Canada
[f] TauRx Therapeutics Ltd., 395 King Street, Aberdeen AB24 5RP, UK

ARTICLE INFO

Keywords:
Mouse model
Parkinson's disease
α-Synuclein
Synaptosomes
Glutamate
Hydromethylthionine

ABSTRACT

The accumulation of alpha-synuclein (α-Syn) into Lewy bodies in cortical and subcortical regions has been linked to the pathogenesis of synucleinopathies such as Parkinson's disease (PD) and dementia with Lewy bodies (DLB). While there is a strong link between synuclein aggregates and the reduction in dopamine function in the emergence of PD, less is known about the consequences of α-Syn accumulation in glutamatergic neurons and how this could be exploited as a therapeutic target. Transgenic h-α-synL62 (L62) mice, in which synuclein aggregation is achieved through the expression of full-length human α-Syn fused with a signal sequence peptide, were used to characterise glutamatergic transmission using a combination of behavioural, immunoblotting, and histopathological approaches. The protein aggregation inhibitor hydromethylthionine mesylate (HMTM) alone, or in combination with the glutamatergic compounds 3-((2-Methyl-4-thiazolyl)ethynyl)pyridine hydrochloride (MTEP) and memantine, was used to target α-Syn aggregation. We show that accumulation of α-Syn aggregates in glutamatergic synapses affected synaptic protein expression including metabotropic glutamate receptor 5 (mGLUR5) levels and ratio of *N*-methyl-D-aspartate (NMDA) receptor subunits GluN1/GluN2A. The ratio of NMDA receptor subunits and levels of mGLUR5 were both normalised by HMTM in L62 mice. These alterations, however, did not affect glutamate release in synaptosomes derived from L62 mice or behavioural endpoints following pharmacological manipulations of glutamate functions. Our results confirm that HMTM acts in the L62 mouse model of PD as an inhibitor of pathological aggregation of synuclein and show that HMTM treatment normalises both the ratio of NMDA receptor subunits and mGLUR5 levels. These findings support the potential utility of HMTM as a disease-modifying treatment for PD aiming to reduce synuclein aggregation pathology.

Abbreviations: α-Syn, alpha-synuclein; AMPA, alpha-amino-3-hydroxy-5-methyl-4-isoxazole propionic acid receptor; AD, Alzheimer's disease; ChAT, choline acetyltransferase; COX IV, Cytochrome c oxidase subunit 4; DLB, Dementia with Lewy bodies; GluA1, glutamate ionotropic receptor AMPA type subunit 1; GluA2, glutamate ionotropic receptor AMPA type subunit 2; GluA3, glutamate ionotropic receptor AMPA type subunit 3; GluA4, glutamate ionotropic receptor AMPA type subunit 4; GluN1, glutamate ionotropic receptor NMDA type subunit 1; GluN2A, glutamate ionotropic receptor NMDA type subunit 2A; GluN2B, glutamate ionotropic receptor NMDA type subunit 2B; mGLUR, metabotropic glutamate receptor; MTEP, 3-((2-Methyl-4-thiazolyl)ethynyl)pyridine hydrochloride; HMTM, N3, N7, N3′, N7′-tetramethyl-10*H*-phenothiazine-3, 7-diaminium bis(methanesulfonate) (leuco-methylthioninium bis(hydromethanesulfonate), hydromethylthionine mesylate; NMDAR, N-Methyl-D-aspartate receptor; PD, Parkinson's disease; PSD-95, Postsynaptic density protein 95; SNARE, N-ethylmaleimide-sensitive factor attachment protein receptor; Syn-1, Synapsin-1; Syn-2, Synapsin-2; Synphy-1, Synaptophysin-1; SNAP-25, Synaptosomal-associated protein, 25 kDa; Sntx-1, Syntaxin-1; VAMP-2, Vesicle-associated membrane protein 2; VGLUT, vesicular glutamate transporter.

* Corresponding authors at: School of Medicine, Medical Sciences and Nutrition, University of Aberdeen, Foresterhill, Aberdeen AB25 2ZD, UK.
E-mail address: g.riedel@abdn.ac.uk (G. Riedel).

https://doi.org/10.1016/j.cellsig.2022.110386
Received 21 March 2022; Received in revised form 7 June 2022; Accepted 8 June 2022
Available online 13 June 2022

1. Introduction

Parkinson's disease (PD) is the most common movement disorder in humans [1]. It is characterised by bradykinesia, rigidity and tremor, and these motor symptoms are related to dopamine depletion caused by a progressive loss of dopaminergic neurones [2]. PD is further associated with a broad spectrum of non-motor symptoms, experienced by most patients, such as cognitive deficits, loss of smell, and depression [3,4]. Alpha-synuclein (α-Syn) has been implicated in regulating synaptic vesicle mobilization and soluble N-ethylmaleimide-sensitive factor attachment protein receptor (SNARE) complex assembly and its regulatory actions are necessary to maintain homeostasis at synapses during intense activity, especially in dopaminergic neurons (reviewed in [5,6]). Increased expression of α-Syn, however, reduces neurotransmitter release and modulates synaptic transmission via neurotransmitter receptor activation [7,8]. The accumulation of α-Syn in Lewy bodies in cortical and subcortical regions has been strongly linked to the pathogenesis of PD [9–11]. While there is unequivocal evidence for a reduction in dopamine function in the emergence of PD, the role of α-Syn aggregation on non-dopaminergic neurotransmitter systems such as glutamatergic, cholinergic, serotonergic, and noradrenergic circuits is less clear [12,13]. Recent evidence suggests that the accumulation of α-Syn aggregates in synaptic terminals precedes neuronal loss and that these α-Syn species impair several steps of synaptic neurotransmission related to synucleinopathies (for review see [14]).

Dysfunction of the glutamatergic synapse has been described for many neurodegenerative disorders [15]. Glutamate is the predominant excitatory neurotransmitter in the mammalian brain and is involved in learning and memory [16]. Once released by the presynaptic endings, it acts mainly on three different post-synaptic receptors: *N*-methyl-D-aspartate receptor (NMDAR), α-amino-3-hydroxy-5-methyl-4-isoxazole propionic acid receptor (AMPAR) and metabotropic glutamate receptors (mGLUR) [17]. Less is known about a fourth class of glutamatergic receptors, the kainate receptors, and recent evidence supports their involvement in epilepsy, schizophrenia, and autism [18]. Excess glutamate in the synaptic space may lead to glutamatergic dysfunction, hyperexcitation and neuronal cell death, as seen in several inflammatory and neurodegenerative disorders [19].

Anomalies in the expression and/or function of the glutamatergic system have been reported in synuclein-related pathologies [20–24]. In mouse brain slices, electrochemical recordings at the level of presynaptic terminals showed that dopamine exerts an important tonic inhibition on glutamate which is essential for regulation of glutamate release [20]. This loss in tonic inhibition in the striatum of PD models may be the underlying cause for alterations in glutamatergic signaling and altered ratios of NMDAR subunits (for review see [15]). Overexpression of α-Syn has been associated with increased phosphorylation of subunits of NMDA and AMPA receptors, further contributing to glutamate toxicity (for review see [21]). In dementia with Lewy bodies (DLB), mGLUR levels were higher in subjects with pure DLB but lower in subjects with DLB-associated with Alzheimer's disease (AD), when compared to control patients [22] and the levels of expression of mGLURs were correlated with the extent of AD pathology [23]. Another study conducted in patients with DLB revealed reduced vesicular glutamate transporter (VGLUT) and postsynaptic density protein 95 (PSD-95) (as well as several GABA receptors) expression in cortical tissue using RNA microarray [24]. These studies suggest that there may be anomalies in the expression and/or function of the glutamatergic system in synuclein-related pathologies.

Previous studies in different α-Syn-based mouse models have reproduced the dopaminergic deficit seen in humans, while we and others have additionally confirmed the accumulation of α-Syn aggregates in glutamatergic pyramidal cells [25–30]. Our L62 mice overexpress the wild-type form of the human α-Syn gene fused to a signal sequence to facilitate aggregation under the control of the mouse *thy1*-promoter. An earlier characterisation of L62 mice using biochemical and pathological methods confirmed the accumulation of proteinase K (PK)-resistant h-α-syn in both the cytoplasm and in synapses in immunohistochemically stained sections, but also in P2 fractions using western blotting (Schwab et al., 2018; Frahm et al., 2018). Different solubility patterns of h-α-syn were revealed through various biochemical extractions and oligomeric synuclein species confirmed by Thioflavin-binding assays. Furthermore, these mice have impaired dopamine and acetylcholine neurotransmission [30,31] and are therefore a useful tool for analysing important aspects of synucleinopathies. The L62 model was used in the present study to examine both glutamatergic function and the effects of targeting α-Syn pathology using the protein aggregation inhibitor hydromethylthionine mesylate (HMTM) either alone or in combination with glutamatergic compounds. We report that α-Syn aggregates accumulate in glutamatergic synapses in L62 mice and cause an increase in mGLUR5 and a loss of correlation between the NMDA receptor subunits GluN1/GluN2A. We further report that treatment with HMTM normalised both the ratio of NMDA receptor subunits and mGLUR5 levels. However, in the L62 model neither synuclein aggregation nor treatment with HMTM had any impact on synaptosomal glutamate release. Likewise, glutamate modulators 3-((2-methyl-4-thiazolyl)ethynyl)pyridine hydrochloride (MTEP), and memantine had little effect on behavioural endpoints in L62 in the presence or absence of HMTM.

2. Materials and methods

2.1. Animals and study design

All animal experiments were performed in accordance with the European Communities Council Directive (63/2010/EU) and approved by the German Animal Research Ethics Committee of LAGESO (Experiments I-III) or the UK Animals Scientific Procedures Act (1986) (Experiment IV) and comply with the ARRIVE guidelines 2.0 [32]. L62 mice have been behaviourally phenotyped using different behavioural paradigms and their dopamine and acetylcholine status revealed using in vivo microdialysis [30,31].

Male and female homozygous L62 and C57BL6/J wild-type litters were bred commercially in individually ventilated cages (Forschungseinrichtung fuer Experimentelle Medizin (FEM), Berlin, Germany) and delivered by truck/plane to the experimental facilities in Berlin (Germany) or Aberdeen (UK) at least 7 days prior to commencement of experimental work. They were housed by genotype and sex in small colonies up to 6 mice in open housing (Macrolon type III) with corncob bedding, paper strips and cardboard tubes as enrichment (cleaning once per week). Holding rooms were at constant temperature (20–22 °C), humidity (60–65%), and air exchange rates (17–20 changes/h) with 12 h light/dark cycle (lights on at 6 am Berlin/ 7 am Aberdeen) and animals had free access to food and water. Mice were 4–6 months of age at experimental start. An overview of animal details, drug treatments, and experimental layouts is given in Table 1.

Four different experiments were conducted: In Experiment I (12 wild-type and 12 L62 male subjects; $n = 6$ per group), mice received HMTM or vehicle, and selected synaptic proteins were analysed in synaptosome-enriched pellet fractions (Figs. 1–4). In Experiment II (48 wild-type and 41 L62 male subjects; $n = 9$–12 per group), mice were treated with HMTM/vehicle and additionally with a single dose of MTEP and underwent behavioural testing in the open field (Fig. 5). In Experiment III (47 wild-type and 45 L62 male subjects; $n = 11$–12 per group), mice were administered HMTM/vehicle together with memantine dissolved in the drinking water and were tested behaviourally in the light dark box (Fig. 6). In Experiment IV (15 wild-type and 12 L62 female subjects), mice did not receive any drug treatment, and synaptic glutamate release was assessed in enriched functional synaptosomes (Fig. 7). Mice were assigned to different study cohorts based on their body weight with equal average body weight for each group at the start of experiments.

Table 1
Study groups and cohort sizes. OF: open field, LDB: light dark box, MEM: memantine. n: number of mice.

Experiment I (HMTM - Synaptic proteins) - Figs. 1–4					
Sex	Age at start	Genotype	n vehicle	n HMTM	n total
Male	6 months	wild-type	6	6	12
		L62	6	6	12

Experiment II (HMTM and MTEP - OF) - Fig. 5							
Sex	Age at start	Genotype	n vehicle + saline	n vehicle + MTEP	n HMTM + saline	n HMTM + MTEP	n total
Male	4 months	wild-type	12	12	12	12	48
		L62	9	11	11	10 (9*)	41 (40*)

Experiment III (HMTM and MEM - LDB) - Fig. 6							
Sex	Age at start	Genotype	n vehicle + water	n vehicle + MEM	n HMTM + water	n HMTM + MEM	n total
Male	4 months	wild-type	12	11	12	12	47
		L62	11 (10*)	11	12 (11*)	11	45 (43*)

Experiment IV (Glutamate release) - Fig. 7				
Sex	Age at start	Genotype	n (±EGTA)	n total
Female	6 months	wild-type	15 (13*)	15 (13*)
		L62	12	12

* Actual n included for behavioural/glutamate release analyses after removal of outliers identified by Grubb's test.

Power calculations were originally conducted using the power calculator tool http://www.anzmtg.org/stats/PowerCalculator/PowerANOVA that was available online at the time these studies were planned with alpha = 0.05, beta = 0.2, effect size delta = 0.5 and power = 0.8 settings. We recently verified them with https://www.stat.ubc.ca/~rollin/stats/ssize/n2.html. Experimenters for behavioural testing, glutamate release studies and histopathology were not blinded to genotype/treatment details. Experimenters for protein quantification studies were blinded to drug treatment details.

2.2. Drugs and treatments

N3,N7,N7′,N7′-Tetramethyl-10*H*-phenothiazine-3,7-diaminium bis (methanesulfonate) (leuco-methylthioninium bis(hydromethanesulfonate); hydromethylthionine mesylate; HMTM) was supplied by TauRx Therapeutics Ltd., Aberdeen, UK at a purity >99% (Exp. 1 & 3: batch 800234810; Exp. 2: batch 7580CL-15). Treatment cohorts were dosed with HMTM or vehicle (argon-sparged deionised water) via oral gavage at a volume of 5 ml/kg body weight. Gavaging was performed in the morning between 8 and 10 a.m. for 5 days per week (Monday-Friday) at a dose of 5 mg/kg HMTM or vehicle. HMTM was prepared daily and administered within 20 min of dissolution in vehicle. Chronic treatment with HMTM lasted up to 7 weeks. HMTM was used alone (Experiment I), with 3-((2-Methyl-4-thiazolyl)ethynyl)pyridine hydrochloride (MTEP) (Experiment II) or with memantine (Experiment III) as stated above.

MTEP was supplied by Tocris Bioscience (Bristol, UK, #2921, batch No. 1). MTEP is a selective mGLUR5 antagonist [33]. Treatment cohorts were dosed intraperitoneally with MTEP or saline (Experiment II). Immediately after injection, mice were released into the open field for behavioural testing (see below). MTEP was administered at 5 ml/kg body weight at a dose of 2.5 mg/kg, and the control group was treated with saline (0.9% *w/v*). MTEP solution was prepared fresh in saline shortly before administration. The concentration of MTEP administered was based on previous work indicating induction of hyperlocomotion in mice at this concentration [34].

Memantine hydrochloride (memantine) was purchased from Tocris Bioscience (#0773, batch No. 5). It is a widely used anti-AD treatment acting via inhibition of NMDA receptors [16]. Memantine was administered orally in the drinking water at a dose of 20 mg/kg body weight (Experiment III). The control group received drinking water without memantine. Based on the approximate daily water intake of 5 ml per mouse, and an average mouse body weight of 25 g, memantine solutions were prepared at a concentration of 0.1 mg/ml. Solutions were prepared twice a week in the morning based on the stability of memantine in water at room temperature [35]. Chronic treatment with memantine continued for 5 weeks. Previous studies have shown that 20–30 mg/kg/day oral administration of memantine via drinking water in mice produces a therapeutically relevant plasma concentration with of about 1 μmol [36–39].

2.3. Behavioural testing in the open field and the light dark box

The open field arena consisted of a grey Perspex square (43 cm × 23 cm × 40 cm: L x W x H), was placed 75 cm above the ground and surrounding cues were obscured by white curtains. Mice were released at the centre of the arena and allowed to move freely for up to 30 min. Movement was recorded by a monochrome overhead CCTV camera (sampling rate 12 Hz). Raw video files were stored as Moving Picture Experts Group (MPEG), and analysed using EthoVision XT10 (Noldus IT, Wageningen, Netherlands). The overall activity (distance moved in cm) was extracted and analysed as the primary readout.

The light dark box was composed of a grey Perspex box (43 cm × 26 cm × 26 cm: L x W x H), placed 75 cm above the ground and surrounded by white curtains. The box was divided into two equal-sized areas separated by a partitioning wall containing an aperture to enable free access to either side. One compartment, the dark zone, was covered by a lid while the *se*cond one remained open and represented the light zone. Mice were released in one corner of the light zone and allowed to explore both compartments freely for 10 min. Ambulation within the light compartment was recorded by a monochrome overhead CCTV camera (sampling rate 12 Hz), raw data files were stored as MPEG, and analysed using EthoVision XT10. The distance moved (cm), the time spent (s) and the velocity cm/s) in the light compartment were extracted as primary readouts for analysis.

Between animals, arenas were cleaned using 70% ethanol before

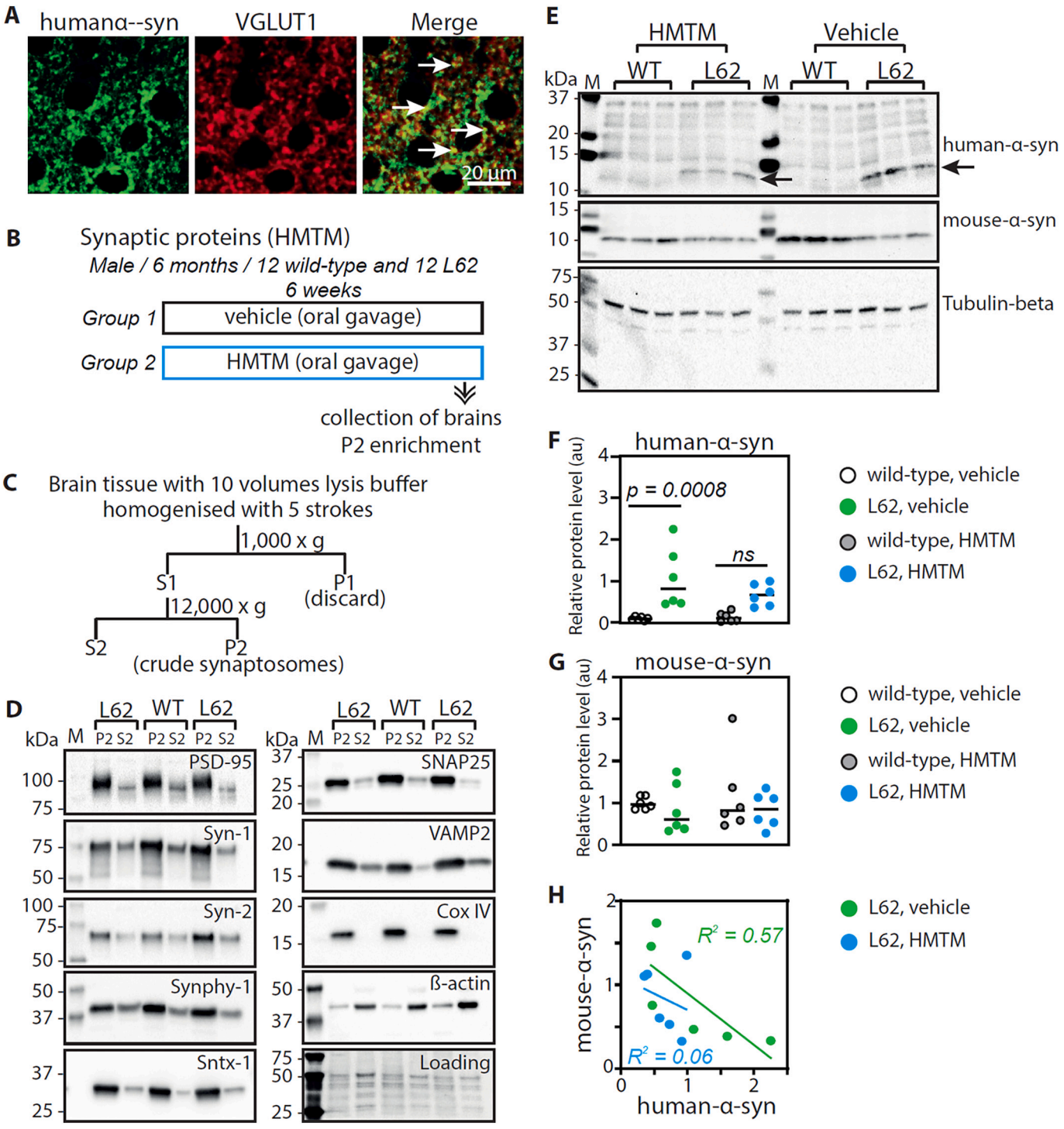

Fig. 1. Human α-Syn is expressed in glutamatergic synapses in L62 mice and is decreased in crude synaptosomes by HMTM. Human-α-Syn (green) co-localises with the presynaptic glutamatergic marker VGLUT1 (red), seen as yellow puncta in the merged image of the immunofluorescence micrographs taken from striatal sections (A). To investigate the influence of HMTM on human- α-Syn and other synaptic proteins of interest, wild-type and L62 mice were administered with HMTM for 6 weeks, and at the end of the study brains collected for extraction of P2 (B). Details of the study are shown in Table 1. For biochemical analyses, crude synaptosomes were extracted using the illustrated protocol (C) detailed in the methods. The enrichment of the crude synaptosomes was verified by labelling of the resulting fractions S2 and P2 with antibodies against selected synaptic proteins, that were separated by Tris-glycine SDS-PAGE (D). For quantification of α-Syn in P2, proteins were separated by Tris-tricine SDS-PAGE; representative blots for human- and mouse-α-Syn are shown (E, arrow indicates α-Syn monomer) and quantification of human- (F) and mouse- α-Syn (G) in these crude synaptic fractions from wild-type and L62 mice, treated with either vehicle or HMTM are illustrated. Densitometric quantification of blots was conducted using the Image Lab software and normalised to beta-tubulin. Individual values and group means are plotted, and statistical analyses were conducted using unpaired *t*-test. Additionally, a correlation analysis was performed between human- and mouse-α-Syn (H) for L62 mice receiving either vehicle (green) or HMTM (blue). α-syn: α-synuclein, WT: wild-type, M: molecular weight marker. Number of mice per group = 6.

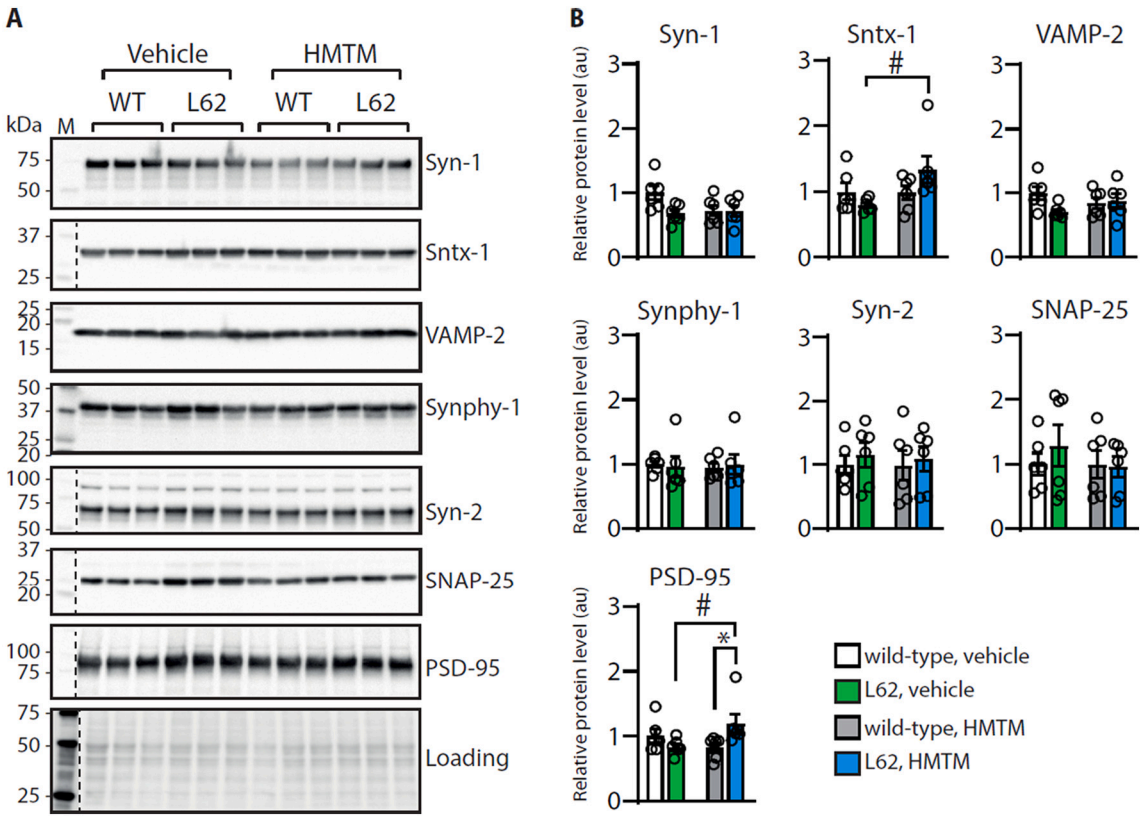

Fig. 2. Abundance of structural proteins in the synapse in wild-type and L62 mice treated with and without HMTM. The proteins derived from P2 crude synaptic fractions from wild-type and L62 mice, treated with vehicle/HMTM were separated by Tris-glycine SDS-PAGE, and representative blots are shown (A). The antibody details are specified in Table 2. Densitometric quantification of synapsin-1 (Syn-1), syntaxin-1 (SNTX-1), VAMP2, synaptophysin-1 (Synphy-1), synapsin-2 (Syn-2), SNAP-25 and PSD-95 was conducted using the Image Lab software and normalised to total protein loading. Individual values, and group mean ± S.E are plotted, and statistical analyses were performed using 2-way ANOVA with genotype and treatment as independent variables. WT: wild-type, M: molecular weight marker. Dotted lines indicate where one sample has been excised (loading control). Number of mice per group = 6. $^{*}p < 0.05$ Bonferroni's multiple comparisons test between L62-HMTM and wild-type-HMTM, $^{\#}p < 0.05$ Bonferroni's multiple comparisons test between L62-HMTM and L62-vehicle.

introducing the next subject. Behavioural assessments took place during the last week of drug dosing between 9 am and 3 pm and mice were sacrificed one to two hours after the last drug administration where applicable.

2.4. Animal sacrifice and collection of brain tissue

Mice were 5–7 months when sacrificed by cervical dislocation. The top of the skull was exposed, and the overlying bone plates removed to allow harvest of the brain in an intact state. Brains were then rapidly extracted, the cortex dissected and snap frozen in liquid nitrogen for protein expression studies (Experiment I) or immediately processed further (excluding olfactory bulbs and cerebellum) for preparation of functional synaptosomes as described below (Experiment IV). For histopathological studies (Experiment III), brains were fixed overnight at room temperature (RT) in 10% (*v*/v) neutral-buffered formalin, embedded in paraffin and sectioned on a rotary microtome (HM 325, Leica Biosystems, Wetzlar, Germany) at 5 μm thickness.

2.5. Immunohistochemistry and manual counting of choline acetyltransferase (ChAT) -positive neurones

Coronal brain sections, 5 μm thick, were collected from front brain areas (corresponding to sections Bregma +0.74 mm for striatum of the mouse brain atlas [40] using a rotary microtome (HM 325, Leica Biosystems), mounted onto glass slides (three sections per slide), deparaffinised, boiled for antigen retrieval in 10 mM citric buffer, pH 6.0, and then incubated in 0.3% (v/v) hydrogen peroxidase solution. Sections were blocked for 20 min in blocking solution (0.1% (*w/v*) bovine serum albumin (BSA) in phosphate buffered saline (PBS), pH 7.4), incubated in primary antibody (anti-choline acetyltransferase (ChAT)), H-95, diluted 1:200, Santa Cruz Biotechnology, Dallas, USA), followed by incubation in biotinylated goat anti-rabbit IgG secondary antibody (Dako Denmark, Glostrup, Denmark). Primary and secondary antibodies were diluted in blocking solution and reactions were conducted for 1 h at RT. Sections were then developed using diaminobenzidine solution (Dako Denmark) and embedded in Neo-Mount (Merck Millipore, Burlington, MA, USA). Images were taken using a light microscope at a 100× magnification (Axio imager M1, Carl Zeiss, Jena, Germany) and ChAT-positive neurones were counted manually in the striatum and the medial septum / diagonal band of Broca (MS/DBB).

2.6. Immunofluorescence

Five-μm coronal sections were collected for striatal areas (corresponding to sections Bregma +0.74 mm, Mouse Brain Atlas [40]) from randomly selected wild-type and L62 mice. The sections were de-waxed, boiled in 10 mM citrate buffer, blocked for 1 h at RT in blocking buffer (5% (*v*/v) normal goat serum in PBS, pH 7.4, containing 0.3% (v/v) Triton X-100) and incubated overnight at 4 °C in primary antibody cocktail (human-α-Syn (Syn 204, Santa Cruz Biotechnology, Dallas, USA), diluted 1:100 and the vesicular glutamate transporter-1 VGLUT1 (#135302 Synaptic Systems, Goettingen, Germany), diluted 1:1000 in blocking buffer). The next day, sections were washed 3 × 10 min with PBS, incubated for 1.5 h at RT in fluorochrome-conjugated secondary antibodies (Alexa Fluor® 488-conjugated donkey anti-mouse IgG and

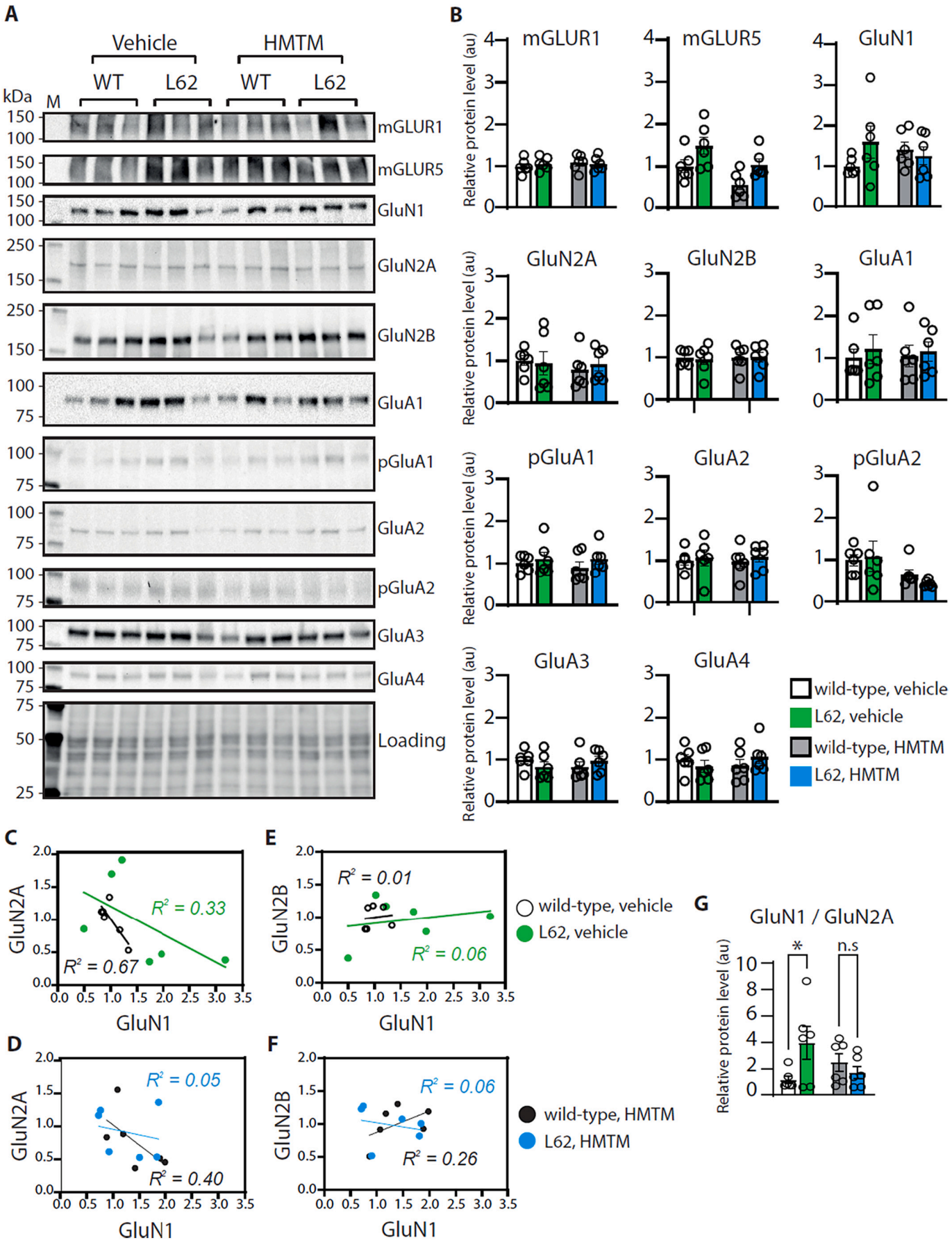

(caption on next page)

Fig. 3. Abundance of glutamatergic proteins in the synapse in wild-type and L62 mice treated with and without HMTM. The proteins derived from P2 crude synaptic fractions were separated by Tris-glycine SDS-PAGE, and representative blots are shown (A). The antibody details are specified in Table 2. Densitometric quantification of the glutamate receptors mGLUR1, mGLUR5, subunits of the NMDA receptor (GluN1, GluN2A and GluN2B), and subunits of the AMPA receptor (GluA1-GluA4, pGluA1 and pGluA2) was conducted using the Image Lab software and normalised to total protein loading. Individual values, and group mean ± S.E are plotted, and statistical analyses were conducted using 2-way ANOVA with genotype and treatment as independent variables. No post-hoc analyses were significant. Additionally, a Pearson correlation analysis was conducted between NMDA receptor subunits GluN1 and GluN2A (C&D) as well as GluN1 and GluN2B (E&F) for vehicle-treated wild-type and L62 mice (C&E), as well as for HMTM-treated cohorts (D&F). The ratio between GluN1 and GluN2A is additionally shown (G). WT: wild-type, M: molecular weight marker. Number of mice per group = 6.

Alexa Fluor® 568-conjugated goat anti-rabbit IgG, Thermo Fisher Scientific, Waltham, MA, USA; both diluted 1:500 in blocking buffer), washed again 3 × 10 min with PBS, covered with Gold Antifade Reagent (Cell Signaling Technology, MA, USA) and examined using a microscope equipped for fluorescence (Axio imager M1).

2.7. Protein extraction, electrophoresis, and immunoblotting

Crushed frozen cortical brain tissue (200 ± 25 mg) was mixed with 1500 μl ice-cold lysis buffer (5 mM HEPES, pH 7.4, 0.32 M sucrose, cOmplete protease-inhibitor cocktail tablets, and PhosSTOP phosphatase-inhibitor cocktail tablets) and homogenized with a tissue homogeniser (T25, IKA, Staufen, Germany) with 5 strokes on level 1 for 15 s each stroke [41]. The homogenate was then centrifuged for 10 min at 1000 x*g* and 4 °C. The pellet (P1) was discarded, and the supernatant (S1) centrifuged for 20 min at 12,000 x *g* and 4 °C. The resulting second supernatant (S2) and pellet containing the crude synaptosomes (P2) were used for further analyses (see Fig. 1). P2 was suspended in 500 μl PBS, pH 7.4 (137 mM NaCl, 2.7 mM KCl, 10 mM Na_2HPO4, 1.8 mM KH_2PO4, cOmplete protease-inhibitor cocktail tablets, and PhosSTOP phosphatase-inhibitor cocktail tablets). The protein concentration was determined using the Bradford reagent (Carl Roth, Karlsruhe, Germany) according to the manufacturer's description. Both fractions were diluted to a final concentration of 5 μg/ μl (P2 in PBS, around 750 μl final volume; S2 in lysis buffer, around 1300 μl final volume), aliquoted to avoid multiple thawing/freezing cycles and stored at −20 °C. S2 and P2 were used to confirm enrichment of synaptosomes. Thereafter, P2 was used to quantify synaptic proteins in brain tissue derived from Experiment I.

Samples (20 μg per lane) were subjected to tricine or glycine SDS-PAGE. The tricine gels (10%) were run using a discontinuous buffer. The cathode buffer consisted of 100 mM Tris, 100 mM tricine and 1% (*w/v*) SDS and the anode buffer contained 100 mM Tris and 0.07% (*v/v*) HCl. The glycine gels (stain-free gradient gels, 4–15%, Bio-Rad Laboratories, Feldkirchen, Germany) were run in Tris-glycine-buffer containing 192 mM glycine, 25 mM Tris and 0.9% (w/v) SDS.

Proteins from glycine gels were transferred to PVDF membranes for 30 min at constant 5 V in Towbin transfer buffer (25 mM Tris, 200 mM glycine, 0.1% (w/v) SDS and 20% (*v/v*) ethanol). Proteins from tricine electrophoresis were transferred to PVDF overnight at 4 °C and 0.4 mA/ cm^2 in tricine transfer buffer (300 mM Tris, 6% (v/v) acetic acid, pH 8.6). Afterwards, membranes were blocked for 1 h at RT in blocking solution (4% (w/v) BSA in TBS with 0.2% (v/v) Tween-20), incubated overnight at 4 °C in primary antibody, diluted in blocking solution, washed 3 times 10 min in TBS-T (TBS with 0.2% (v/v) Tween-20) and incubated for 1 h at RT in appropriate secondary antibody diluted in blocking solution. After washing 3 more times in TBS-T, membranes were overlaid for 1 min with ECL solution (100 mM Tris pH 8.5, 1.25 mM luminol, 200 μM *p*-coumaric acid, 0.01% (v/v) H_2O_2). The chemiluminescence signals were detected by the ChemiDoc Imaging System (Bio-Rad Laboratories), and the Image Lab software (version 6.1, Bio-Rad Laboratories) applied for densitometric quantification. The membranes from tricine gels were labelled with antibodies against human-α-Syn and mouse-α-Syn, and additionally with beta-tubulin as loading control for normalisation. The membranes from glycine gels were used for all other antibodies and total protein loading (stain-free gels) was used for normalisation. Details of antibodies used are given in Table 2.

2.8. Glutamate release

Naïve mice were killed by cervical dislocation and the brains carefully removed in an intact state to extract synaptosomes [41,42]. Whole brains were quickly rinsed in 20 ml ice-cold sucrose/EDTA/tris solution (0.32 M sucrose, 1 mM EDTA, 5 mM tris, pH 7.4), transferred to another tube with 10 ml fresh sucrose/EDTA/tris solution and briefly minced with scissors. The tissue was then homogenized with seven strokes at 700 rpm (Eurostar 20 homogeniser, IKA, Staufen, Germany), spun in a pre-cooled 50 ml centrifugation tube for 10 min at 2800 x*g* and 4 °C. The supernatant (S1) was removed and kept on ice; the pellet was suspended with 10 ml sucrose/EDTA/tris, centrifuged for a further 10 min at 2800 x *g* and 4 °C and the second supernatant (S2) pooled with the first supernatant. Combined supernatants S1 and S2 were centrifuged for 15 min at 13,000 x *g* and 4 °C and the final pellet (P2) suspended in 6 ml ice-cold Krebs solution (118.5 mM NaCl, 4.7 mM KCl, 1.2 mM $MgSO_4$, 10 mM glucose, 1 mM Na_2HPO_4, 20 mM HEPES, pH 7.4). The protein concentration in P2 was determined using the Lowry method (Bio-Rad) according to the manufacturer's description. The synaptosome solution was then diluted in Krebs solution to a final concentration of 0.6 mg/ml and used for the glutamate release assay.

For glutamate release, a potassium (K^+) chloride dependent enzyme-linked assay was used. Synaptosomes (0.6 mg in 2 ml) were diluted in Krebs solution, either in the presence of Ca^{2+} (0.4 mM $CaCl_2$) or in its absence (including 1 mM EGTA (ethylene glycol-bis (β-aminoethyl ether)-N,N,N′,N′-tetraacetic acid, Sigma-Aldrich). Enzymatic reactions were carried out at 37 °C in 3.5 ml flat-bottomed cuvettes (Starna Scientific Ltd) on an 8 mm magnetic stirrer (Fisher Scientific, UK) in the sample chamber of the spectrofluorometer (Photo Technology International DeltascanTM Model 4000–45). Experiments were started at t = 0 mins by the addition of $NADP^+$ (1 mM; Sigma-Aldrich, Burlington, MA, USA) to synaptosomes. Once the synaptosome suspension was equilibrated, glutamate dehydrogenase (50 U/ml) was added at t = 60 mins and glutamate release initiated by KCl (30 mM) at t = 240 mins. Fluorescence recordings took place using λex = 340 nm, λem = 460 nm. In general, all experiments followed the same timeline and control L-glutamate (0.5 mM) was added at t = 660 mins and recordings terminated at t = 900 mins. Data were continuously collected (1 Hz sampling rate) and original traces saved in ASCII format (Lab Master Series Software, version 1.22, 1986; Scientific Solutions Inc., Mentor, OH, USA) and exported to Microsoft Excel. The raw absorbance values were then converted to glutamate release (according to 0.6 mg/ml per synaptosome) and all traces were aligned to 240 min. Next, values at t = 660 min to t = 900 min in the presence of external 0.5 mM glutamate standard were quantified and then normalised to fluorescence derived from wild-type mice. Maximal release was calculated from t = 660 minus those from t = 240 for K^+-evoked glutamate release. To reduce noise artefacts, traces were smoothed, using 2nd order polynomial smoothing (GraphPad Prism software version 8.00; GraphPad Software Inc., San Diego, CA, USA).

2.9. Data analyses

For immunoblotting and behavioural data, individual values, group mean, and S.E. (standard error) were plotted. Glutamate release data is shown as smoothed traces over 900 s and cumulative maximal release as group mean and S.E. Statistical analyses were conducted using 2-way or

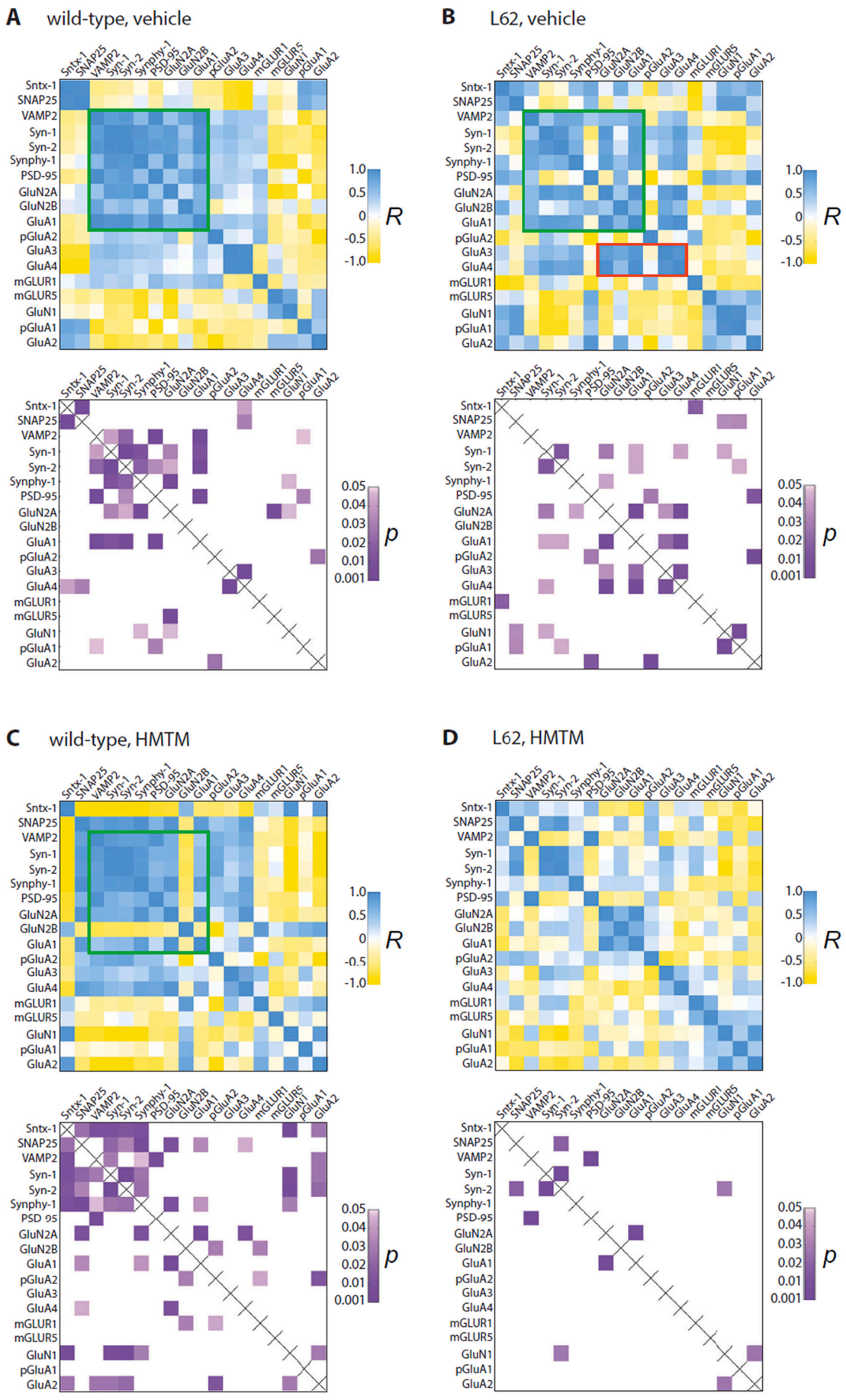

(caption on next page)

Fig. 4. Pairwise correlation analyses of synaptic proteins in wild-type and L62 mice treated with and without HMTM. Heatmaps for Pearson's pairwise correlations (blue and yellow) and the resulting *p*-values (purple) are shown for vehicle-treated wild-type (A) and L62 mice (B), as well as for HMTM-treated wild-type (C) and L62 mice (D). R-values in the correlation heatmaps are displayed blue for positive correlations and yellow for negative correlations; where a correlation is lacking (R close to 0), then cells are white. Corresponding p-values were coloured purple if significant ($p < 0.05$) and lack of significancy is shown in white. The correlations were performed pairwise between the synaptic proteins Syn-1, Syn-2, Synphy-1, Sntx-1, SNAP-25, VAMP-2, PSD-95, mGLUR1, mGLUR5, GluN1, GluN2A, GluN2B, GluA1, pSer845-GluA1, GluA2, pTyr869-GluA2, GluA3 and GluA4. For the cells identified within the green square in A, B and C, strong positive correlations were particularly obvious between presynaptic structural proteins including synapsins and synaptophysin and post-synaptic proteins such as PSD-95 and NMDA receptor subunits GluN2A and B, as well as AMPA glutamate receptors GluA1 in wild-type mice. Within the red rectangle in B, there was a high positive correlation for GluA3/4 with some NMDA receptor subunits such as GluN2A/B, GluA1, GluA3 and GluA4 in L62 mice.

3-way analysis of variance (ANOVA) with Bonferroni multiple comparison correction post-hoc test or unpaired *t*-test where appropriate. Further, correlation analyses using Pearson correlation between the synaptic proteins (raw expression values) were conducted. Outliers were identified by Grubb's test and a total of five outliers (Table 1) were identified: one outlier in Experiment II (one L62 receiving HMTM and MTEP), two in Experiment III (one L62 receiving vehicle and drinking water, and one L62 receiving HMTM and drinking water), and two outliers in Experiment IV (two wild-type). GraphPad Prism software (version 8.00; GraphPad Software Inc.) was applied for all statistical analyses and for generation of graphs and heatmaps. Differences were considered significant at $p < 0.05$ and only significant outcomes are reported in the text.

3. Results

3.1. The abundance of human-α-Syn monomers is increased in L62 crude synaptic fractions

We have previously reported that L62 mice show widespread human-α-Syn immunoreactivity in brain and spinal cord, with several neuronal populations having high expression levels, including glutamatergic and cholinergic neurones in cortex and striatum [30,31]. We now show that human-α-Syn also accumulates in glutamatergic synapses. Labelling of frontal brain sections with antibodies against human-α-Syn (green) and VGLUT1 (red), a marker for glutamatergic synapses, shows co-localisation of both proteins as yellow puncta in the merged image (Fig. 1A). In Experiment I (Fig. 1B) we measured the levels of human-α-Syn accumulation in crude synaptosomal fractions obtained from brain extracts following the procedure depicted in Fig. 1C in L62 and wild-type mice with and without HMTM treatment. Enrichment of synaptosomes in P2 was confirmed for several presynaptic markers (e.g., synapsin-1, syntaxin-1, SNAP-25, and others), as well as the post-synaptic marker PSD-95 and the mitochondrial marker Cox IV (Fig. 1D). On the other hand, beta-actin was significantly reduced in the P2 and enriched in the S2 fraction (Fig. 1D). Additional calibration experiments to permit quantification and measurement of these proteins are shown in Supplementary Fig. 1. Within the tested range of protein loading (up to 20 μg), linearity was confirmed for reactivity with the antibody at the dilutions applied. A total protein loading of 20 μg was chosen to quantify the synaptic proteins of interest and the corresponding dilutions of the different antibodies are provided in Table 2. Quantitative analysis of representative immunoblots (Fig. 1E) confirmed the expected increase in human-α-Syn in vehicle-treated L62 mice relative to wild-type litters. Treatment with HMTM at 5 mg/kg reduced human-α-Syn immunoreactivity to levels seen in wild-type mice (Fig. 1F). Mouse-α-Syn levels were not affected by HMTM (Fig. 1G). Interestingly, there was a near significant negative correlation between human-α-Syn and mouse-α-Syn in L62 mice receiving vehicle (Fig. 1H, correlation coefficient $R^2 = 0.57$ and $p = 0.08$), but not in HMTM-treated L62 mice (Fig. 1H, correlation coefficient $R^2 = 0.06$ and $p = 0.64$). Changes in body weights did not differ between cohorts after the 6 weeks treatment with HMTM (Supplementary Fig. 2A).

3.2. The abundance of synaptic proteins and subunits of glutamate receptors is different in crude synaptic fractions from L62 mice

Levels of several proteins involved in structural (pre-synaptic, Fig. 2) and glutamate signaling functions (post-synaptic, Fig. 3) were examined in the same P2 fractions (Experiment I, see Fig. 1B). There were no differences between groups in levels of synapsin-1, VAMP-2, synaptophysin-1, synapsin-2, or SNAP-25 (Fig. 2A). There was an interaction effect for syntaxin-1 (genotype x treatment $F(1,20) = 4.427$; $p = 0.048$, Fig. 2B) indicating an increase in syntaxin-1 only in L62 mice following HMTM treatment (see hashtag, Fig. 2B). Similarly, PSD-95 was increased only in L62 following HMTM treatment (genotype x treatment $F(1, 20) = 7.179$; $p = 0.014$, Fig. 2B, see hashtag relative to L62 vehicle, and see asterisks for comparison with HMTM-treated wild-type mice).

As shown in Fig. 3A, the majority of glutamatergic proteins examined did not differ between genotypes and treatments. However, L62 mice had significantly elevated levels of mGLUR5 (main effect of genotype $F(1, 20) = 9.870$; $p = 0.005$, Fig. 3B). Treatment with HMTM decreased mGLUR5 in both wild-type and L62 mice (main effect of treatment $F(1, 20) = 8.487$; $p = 0.009$, Fig. 3B). Furthermore, HMTM decreased the phosphorylation levels of AMPA subunit GluA2 in both wild-type and L62 mice similarly (main effect of treatment $F(1, 20) = 6.394$; $p = 0.020$, Fig. 3B). Interestingly, there was a significant negative correlation between NMDA receptor subunits GluN1 and GluN2A in vehicle-treated wild-type mice (Fig. 3C, correlation coefficient $R^2 = 0.67$ and $p = 0.045$), while no correlation was seen in vehicle or HMTM-treated L62 mice (Fig. 3C–D, correlation coefficient $R^2 = 0.33$ and $p = 0.233$ for vehicle-treated L62 and $R^2 = 0.05$ and $p = 0.66$ for HMTM-treated L62). Levels of NMDA receptor subunits GluN1 and GluN2B were unaffected either by genotype or treatment (Fig. 3E–F). Nevertheless, the ratio of NMDA receptor subunits GluN1 and GluN2A was normalised in L62 by HMTM treatment (genotype x treatment $F(1, 20) = 18.91$; $p = 0.029$, and asterisks for post-test Fig. 3G).

We used heatmapping to display the strength of statistical significance of pairwise correlations according to genotype and HMTM treatment. The findings are depicted in Fig. 4, in which the two vehicle conditions (Fig. 4A and B) and the two genotypes treated with HMTM (Fig. 4C and D) are compared. In wild-type mice, strong positive correlations were particularly obvious between presynaptic structural proteins, including synapsins and synaptophysin, and post-synaptic proteins, such as PSD-95 and NMDA receptor subunits GluN2A and GluN2B, as well as AMPA glutamate receptors GluA1 (see green square in Fig. 4A). Many of these correlations were significant (see bottom graph of Fig. 4A). The correlations were maintained in wild-type mice treated with HMTM (Fig. 4C), and in many instances correlations were increased or even emerged, most prominently for SNAP-25 and other synaptic proteins. Correlations for GLURs became positive and for syntaxin-1 became strongly negative following HMTM treatment. Importantly, GluN2 correlations were lost following HMTM treatment and were replaced by correlations for other Glu species (GluA3, GluA4 and pGluA2). By contrast, all other Glu receptor subunits showed either weak or negative correlations with presynaptic proteins, and between each other.

The pairwise correlational relationships were less organised and much weaker in L62 mice, with few showing statistical significance

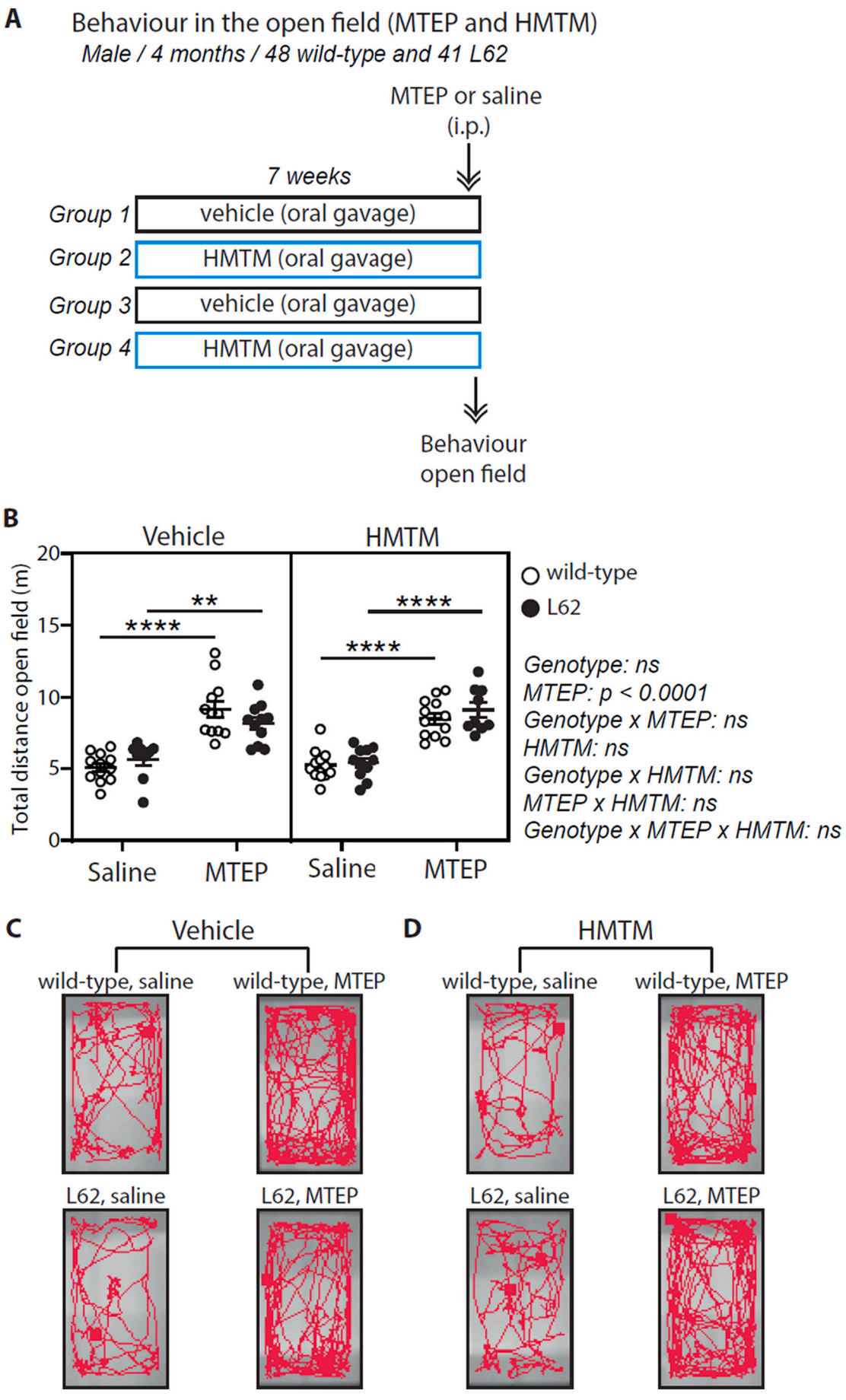

(caption on next page)

Fig. 5. Acute treatment with the mGLUR5 receptor antagonist, MTEP, increases locomotor activity in wild-type and L62 mice and HMTM does not interfere with this locomotor activation. To investigate the influence of MTEP and HMTM on the locomotor behaviour, a drug study with wild-type and L62 mice was conducted. Mice received HMTM for 7 weeks and during the last week of HMTM dosing, acute intraperitoneal injections with MTEP or saline were given, and locomotion was assessed in the open field (A). Details of the study are shown in Table 1. The total distance moved in the open field arena was extracted as the primary output and values are shown individually along with the group mean and S.E (B). Statistical analyses were conducted using 3-way ANOVA with genotype, MTEP and HMTM as independent variables, followed by the Bonferroni post-test (** $p < 0.01$ and **** $p < 0.0001$). OF: open field. Number of mice: wild-type vehicle + saline $n = 12$, wild-type vehicle + MTEP n = 12, wild-type HMTM + saline $n = 12$, wild-type HMTM + MTEP n = 12, L62 vehicle + saline $n = 9$, L62 vehicle + MTEP $n = 11$, L62 HMTM + saline n = 11, L62 HMTM + MTEP $n = 9$. Representative video-tracks in the open field of vehicle (C) and HMTM cohorts (D), co-treated with saline/MTEP.

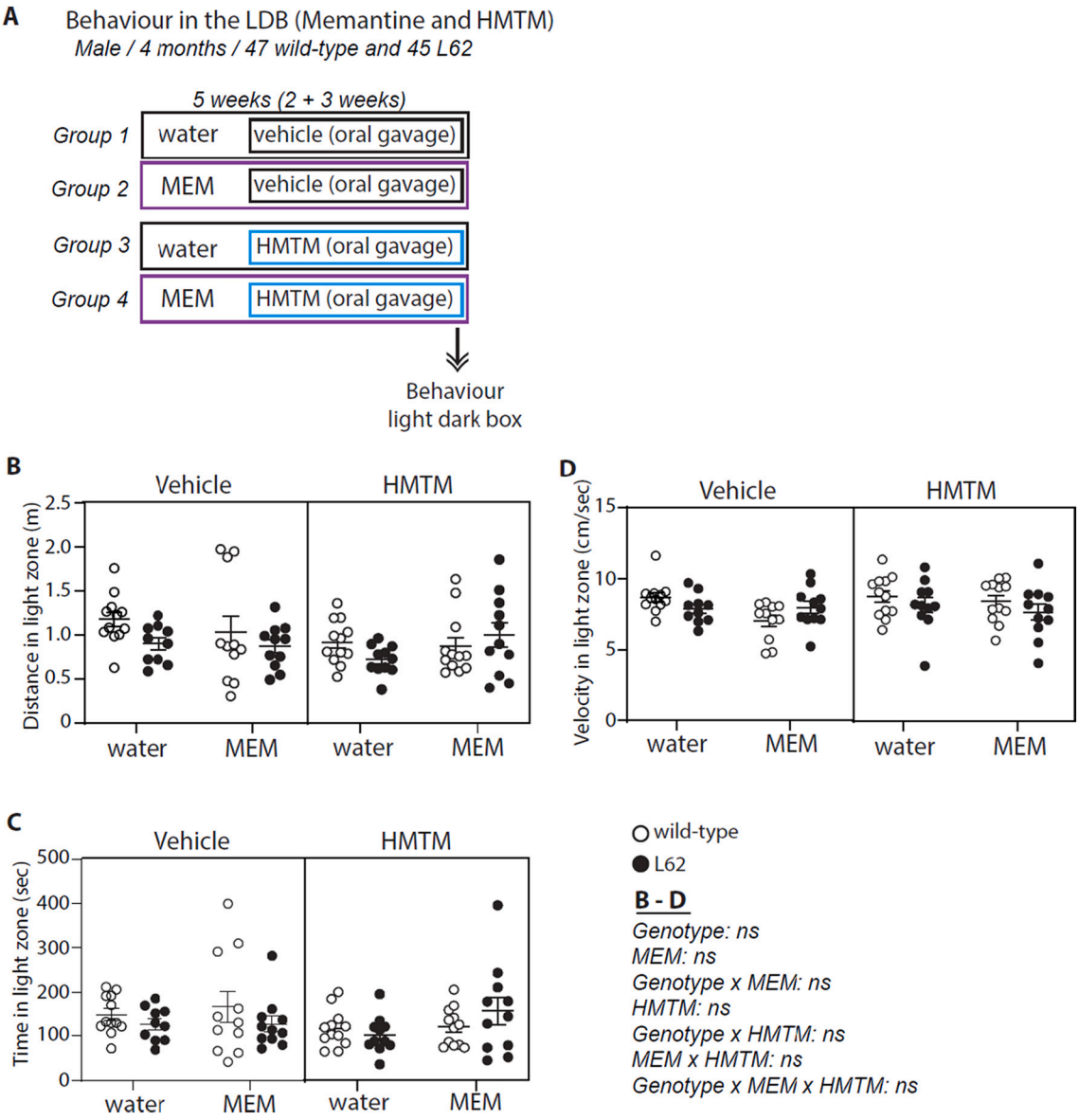

Fig. 6. Chronic treatment with the NMDA receptor antagonist, memantine, does not change anxiety and locomotor activity of wild-type and L62 mice and HMTM has no additional effect to memantine. To investigate the influence of memantine (MEM) and HMTM on locomotion and anxiety, mice received water or memantine in their drinking water for 5 weeks. Additionally, HMTM was given for the last 3 weeks along with memantine. During the last week of dosing, behaviour of mice was assessed in the light dark box (A). Details of the study are shown in Table 1. The distance moved (B), the time (C) and the velocity in the light zone (D) were extracted as primary endpoints and values are presented individually along with the group mean and S.E. Statistical analyses were conducted using 3-way ANOVA with genotype, memantine and HMTM as independent variables. LDB: light dark box, MEM: memantine. Number of mice: wild-type vehicle + water, $n = 12$; wild-type vehicle + MEM, $n = 11$; wild-type HMTM + water, n = 12; wild-type HMTM + MEM, n = 12; L62 vehicle + water, $n = 10$; L62 vehicle + MEM, n = 11; L62 HMTM + water, n = 11; L62 HMTM + MEM, $n = 11$.

(bottom of Fig. 4B). Intriguingly, there is an almost complete loss of correlations for PSD-95, a stabilizer for NMDA receptors [43], with synaptic and other glutamate receptor proteins. On the other hand, there were strong positive correlations for GluA3/4 with some NMDA receptor subunits (see red rectangle in Fig. 4B) in L62 mice. Most of these positive correlations in L62 mice were weakened following HMTM treatment (Fig. 4D) with the correlation map appearing more scattered with few reaching statistical significance.

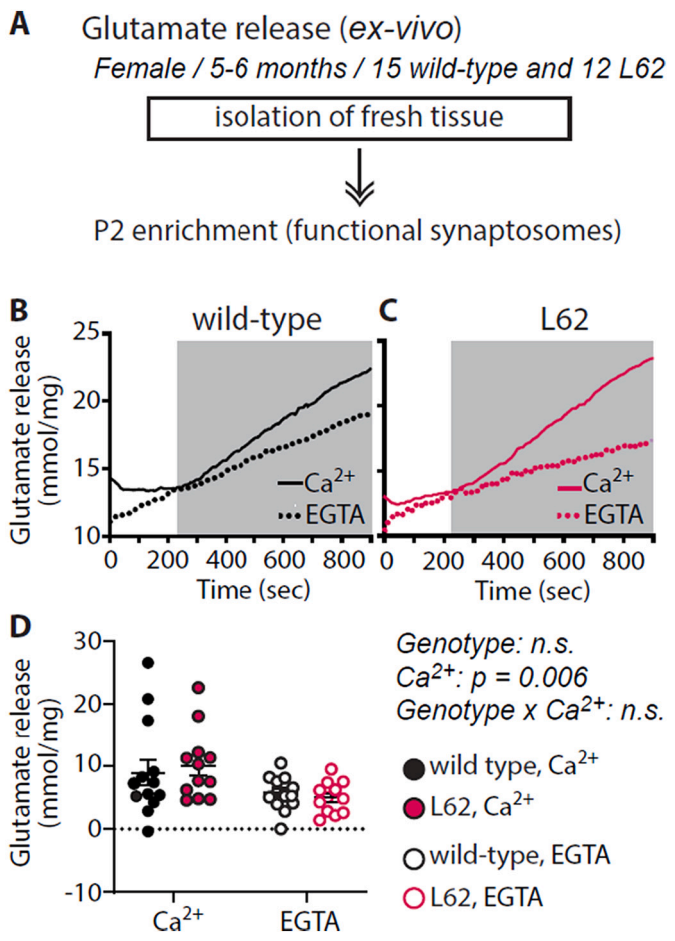

Fig. 7. Synaptic glutamate release in functional synaptosomes is similar between wild-type and L62 mice and depends on the presence of Ca^{2+}. To investigate glutamate release, crude synaptic fractions containing functional synaptosomes were extracted (A) and were used to perform a fluorescence-based assay for glutamate release studies in wild-type (B) and L62 (C) mice, in the presence of Ca^{2+} (continues lines) or its absence (= addition of EGTA, dotted lines). Data in (B) and (C) are shown as smoothed curves with no error bars for a better overview and the shaded area shows the timeframe in which glutamate release was stimulated after potassium chloride administration. Both, wild-type and L62 mice, showed higher glutamate release when Ca^{2+} was present and similarly lower release when EGTA was added to measure the Ca^{2+}-independent glutamate release. Cumulative data for maximal glutamate release for each genotype was extracted, as described in Methods, and individual values, group mean, and S.E. are plotted in (D) and show no differences between wild-type and L62 mice. Statistical analyses were conducted using 2-way ANOVA with genotype and Ca^{2+} as independent variables. Number of mice: wild-type $n = 13$, L62 $n = 12$.

The overall number of significant ($p < 0.05$) or strongly significant ($p < 0.001$) correlations ranked as follows: wild-type + HMTM > wild-type > L62 > L62 + HMTM. We found that the significant correlation between SNTX-1 and SNAP-25/SYN-2, as well as between SNAP-25 and synaptophysin-1 seen in wild-type mice (Fig. 4A) were absent in L62 mice (Fig. 4B). Correlations between the AMPA subunit GluA1 and the remaining AMPA subunits were similar between genotypes but stronger and thus significant between GluA1 and GluA3/4 in L62 (compare red highlighted areas in Fig. 4A and B). Furthermore, there was a significant correlation between PSD-95 and GluA1/phosphoGluA1 in wild-types, which was absent in L62, and instead PSD-95 was found to correlate with GluA2/phosphoGluA2.

In wild-type mice, HMTM exposure particularly enhanced the significance for correlations of structural and functional presynaptic proteins (Fig. 4C) but reduced the correlations between the glutamate receptor subunits. Very few (6 in total) significant correlations remained in L62 mice after long-term exposure to HMTM (Fig. 4D) with no clear pattern emerging.

Table 2
List of antibodies used for immunoblotting.

Primary antibodies	Source	Antibody-ID	Host	Dilution
Human-α-Syn (Syn 204) *#	Santa Cruz Biotechnology	sc-32,280	mouse	1:100
Mouse-α-Syn (D37A6) *#	Cell Signaling Technology	4179	rabbit	1:1000
Beta-tubulin*	Cell Signaling Technology	15,115	rabbit	1:1000
PSD-95	Cell Signaling Technology	3450 T	rabbit	1:1000
Synapsin-1, Klon46.1	Synaptic Systems	106,001	mouse	1:50,000
Synapsin-2	Cell Signaling Technology	85,852	rabbit	1:10,000
Synaptophysin-1	Synaptic Systems	101,002	rabbit	1:10,000
Syntaxin-1	Abcam	ab112198	mouse	1:50,000
SNAP-25	Biolegend	805,001	mouse	1:5000
VAMP-2	Synaptic Systems	104,202	rabbit	1:50,000
COX IV	Cell Signaling Technology	4850	rabbit	1:1000
ß-actin	Santa Cruz Biotechnology	sc-1615	goat	1:5000
mGLUR1	Cell Signaling Technology	12,551	rabbit	1:1000
mGLUR5	Abcam	ab76316	rabbit	1:10,000
GluN1	Cell Signaling Technology	5704	rabbit	1:1000
GluN2A	Cell Signaling Technology	4205	rabbit	1:1000
GluN2B	Cell Signaling Technology	14,544	rabbit	1:1000
GluA1	Cell Signaling Technology	13,185	rabbit	1:1000
pSer845-GluA1	Cell Signaling Technology	8084	rabbit	1:1000
GluA2	Cell Signaling Technology	5306	rabbit	1:1000
pTyr869-GluA2	Cell Signaling Technology	3921	rabbit	1:1000
GluA3	Cell Signaling Technology	4676	rabbit	1:1000
GluA4	Cell Signaling Technology	8070	rabbit	1:1000

Secondary antibodies (HRP-conjugated)	Source	Antibody-ID	Host	Dilution
Goat-anti-mouse	Agilent (Dako)	P0447	goat	1:5000
Goat-anti-rabbit	Agilent (Dako)	P0448	goat	1:5000
Rabbit-anti-goat	Agilent (Dako)	P0449	rabbit	1:5000

* These antibodies were used to label membranes from Tris-tricine gels. All other antibodies were used on membranes from Tris-glycine SDS-PAGE.

We have explored human/mouse selectivity in multiple other commercial (Syn211, LB50, sc-7011R,sc-69977) and in-house antibodies (AB539, AB874, AB736). Due to the high sequence similarity between human and mouse α-Syn, none of them was species-specific.

3.3. *The response pattern in open field and light dark box following challenge with glutamatergic antagonists in L62 mice is normal*

Having established that accumulation of human-α-Syn in glutamatergic synapses in L62 produces a major disruption in the correlations that normally exist between structural proteins of the synapse and glutamate receptors, we went on to explore the functional consequences of these changes using different glutamatergic antagonists: MTEP for

mGLUR5 and memantine for NMDA receptors.

In Experiment II, mice were chronically treated with HMTM (controls received vehicle) for 7 weeks and an acute intraperitoneal injection of MTEP/saline was administered prior to assessment of locomotor activity in the open field arena (Fig. 5A). The selective mGLUR5 antagonist, MTEP, at a dose of 2.5 mg/kg, significantly stimulated ambulatory activity during thirty minutes of free exploration (Fig. 5B). Induction of locomotor hyperactivation by MTEP was comparable between genotypes, both in vehicle and HMTM-treated cohorts (3-way ANOVA: effect of MTEP $F(1, 80) = 131.5$; $p < 0.0001$). These effects are confirmed by representative video-tracks (Fig. 5C/D). Change of body weights at sacrifice did not differ for individual drug treatment groups, but there was an interaction effect for MTEP and HMTM (3-way ANOVA: effect of MTEP x HMTM $F(1, 79) = 5.41$; $p = 0.023$, Supplementary Fig. 2B).

In Experiment III, mice were exposed to memantine-containing or normal drinking water for a total of 5 weeks. During weeks 3–5, an additional daily oral dose of 5 mg/kg HMTM/vehicle was given to selected subgroups followed by behavioural assessment in the light dark box (Fig. 6A). The distance moved, the time spent, and the velocity in the light compartment, recorded via video-observation, were considered primary readouts for locomotion and anxiety in this behavioural paradigm. The distance moved, the time spent in the light zone and the velocity were all similar between treatment groups (Fig. 6B–D). Body weight change at sacrifice (Supplementary Fig. 2C), was significantly different between genotypes and due to treatment with memantine (3-way ANOVA: effect of MEM $F(1, 84) = 57.41$; $p < 0.0001$, effect of genotype $F(1, 84) = 13.61$; $p = 0.0004$, effect of MEM x genotype $F(1, 84) = 22.18$; $p < 0.0001$), and the memantine effect was greater in HMTM-treated cohorts (effect of MEM x HMTM $F(1, 84) = 5.50$; $p = 0.021$). Furthermore, to explore/exclude any effect of memantine on cholinergic tone, we quantified ChAT-positive neurones in basal forebrain regions and the striatum in L62 mice (Supplementary Fig. 3A/B, respectively). The number of cholinergic neurones was similar between L62 cohorts receiving the different drugs, both in MS/DBB (Supplementary Fig. 3C) and in striatum (Supplementary Fig. 3D).

3.4. Glutamate release in functional synaptosomes is intact in L62 mice

Given the lack of difference between wild-type and L62 mice in their behavioural responses to post-synaptically active glutamatergic antagonists, we examined glutamate release in synaptosomes prepared from naïve mouse brain tissues using a fluorochrome-based kit (Experiment IV, Fig. 7A). In wild-type mice, the glutamate release was significantly greater in the presence of Ca^{2+} compared to release when EGTA was added (Fig. 7B, main effect of Ca^{2+}: $F(1, 850) = 2575$; $p < 0.0001$). In L62 mice, the glutamate release was likewise significantly greater in the presence of Ca^{2+} compared to when EGTA was added (Fig. 7C, main effect of Ca^{2+}: $F(1, 850) = 1387$; $p < 0.0001$). Cumulative data show similar maximal glutamate release values for wild-type and L62 mice and confirm the Ca^{2+} dependence (Fig. 7D, main effect of Ca^{2+} $F(1, 46) = 8.36$; $p = 0.006$).

4. Discussion

We have reported previously that the L62 model of synucleinopathy is characterised by widespread accumulation of human-α-Syn in different neuronal populations of the brain including cortex, basal forebrain, striatum, and spinal cord. Synuclein pathology was particularly noted in cholinergic neurons and in glutamatergic pyramidal cells [30]. Treatment with the protein aggregation inhibitor HMTM reduced synuclein pathology in multiple brain regions and reversed some of the anxiety-related traits in these animals [44]. In the present report, we have extended our investigations of the L62 model with a particular focus on the glutamatergic system. We now show that the location of human-α-Syn in glutamatergic neurons is synaptic, and that it is enriched in crude synaptic preparations from the brain of L62 mice. Importantly, we confirm that this elevation in synaptic human-α-Syn is normalised by treatment with HMTM. The results confirm, therefore, that HMTM acts as an inhibitor of synuclein aggregation in the brain and decreases the synaptic load of pathology.

Given the possibility to both induce and reverse synaptic human-α-Syn pathology in L62 mice, we investigated how these changes impact on a range of structural synaptic proteins and glutamatergic receptor proteins. Surprisingly, the levels of structural synaptic proteins examined (synapsin, VAMP2, synaptophysin and SNAP25) were unaffected by human-α-Syn aggregation and/or HMTM administration. Exceptions are the presynaptic SNARE protein syntaxin and the post-synaptic protein PSD-95 that are increased in L62 mice only when HMTM was given. This drug sensitivity in a subset of synaptic proteins suggests a decline in synaptic function rather than synapse loss and is in line with findings from the striatum of transgenic mice overexpressing a truncated human α-Syn (1−120) [45]. Synaptic accumulation of α-Syn was accompanied by an age-dependent redistribution of SNARE proteins SNAP-25, syntaxin-1 and VAMP-2, but no synapse loss [45]. Similarly, syntaxin-1A and VAMP-2 but not SNAP-25 were significantly reduced in extracellular vesicles from peripheral blood from PD subjects compared to controls [46]. Less relevant, but indicative of a similar mechanism, are data from a proteomic study on CSF from AD patients which confirmed increased amounts of syntaxin-1, and VAMP-2 [47], while others reported that syntaxin, SNAP-25 and synuclein showed a biphasic abundance rather than a static decrease/increase in AD brains in response to Braak staging [48]. These data support the idea that remodelling of synaptic proteins is an early response to pathological protein formation in multiple diseases and this process is truthfully mimicked in L62. This is consistent with adaptations in the post-synapse, here measured as altered PSD-95/glutamate receptors, possibly as an indirect response to presynaptic changes in protein expression.

As with the structural synaptic proteins, the levels of most glutamatergic receptor proteins were unaffected by human-α-Syn aggregation. The main exception was a selective increase in mGLUR5 in L62 mice, and the reversal of this effect by HMTM treatment. Similarly, HMTM treatment reduced the levels of the phosphorylated AMPA subunit of GluA2. There is normally a negative correlation between the NMDA subunits (GluN1 and GluN2A) that was absent in L62 mice, and treatment with HMTM normalised the ratio of these subunits although it did not re-establish the correlation. Alterations in mGLUR5 receptor expression and function have been widely reported in α-Syn overexpressing models [92] and it appears to be a specific and crucial step for the induction and progression of α-Syn-mediated pathology and microglia-associated neuroinflammation [93]. The correction of mGLUR5 levels by HMTM therefore constitutes a further beneficial action of the drug. This feature in our model corroborates observations in PET brain images from PD patients also showing heightened mGLUR5 levels [84] and suggests that PD patients may be at risk of hyperexcitation and that downregulation of calcium-activating glutamate channels including mGLUR5 and NMDA – both are achieved by HMTM administration - is a valid treatment strategy to prevent excitotoxicity. The mechanism for this selectivity of adaptations for mGLUR5 and GluN1/2 remains to be defined. Others have suggested that a differential distribution of mGLURs and NMDA receptor subunits in the brain and their compartmentalisation at the synaptic junction e.g., cell-surface vs. extracellular compartment must be considered to understand the selective changes in PD (for review see [49]).

Since the effects of human-α-Syn aggregation on synaptic protein levels are limited in L62 mice, we investigated how their relationships are affected using a pairwise correlation analysis approach. The fine-tuning of the synaptic machinery is needed for proper synaptic functioning and small changes may lead to the synaptic pathology that is often observed in neurodegenerative disorders [50]. Comparison of the significant pairwise correlations seen in wild-type and L62 mice revealed the loss of normal correlations and the emergence of several novel possibly pathological correlations. Notably, there was an almost

complete loss of correlations for PSD-95, a stabilizer for NMDA receptors [43], and other glutamate receptor proteins. These were replaced in L62 mice by abnormal glutamate receptor correlations: GluN2A & GluA4, GluA1 & GluA4, GluA1 & GluN1, and GluA2 & PSD-95. This is the first analysis of this kind published to date and so it is not possible to make comparisons with other reports. However, the importance of differential expression levels and putative correlations of NMDA receptor subtypes has been confirmed for multiple brain regions, diseases, and behavioural responses [51–53]. In our specific analysis, the emergence of novel correlations is most likely an adaptation to the overexpression of human-α-Syn and the progressive accumulation of its aggregated species. Indeed, this causal relationship is underlined by the fact that α-Syn aggregation is inhibited by HMTM and reduced these pathological correlations.

Having shown that human-α-Syn pathology induces a range of abnormalities in glutamatergic proteins and that these can be partially corrected by treatment with HMTM, we investigated how these respond to pharmacological manipulations using two well established glutamatergic antagonists, MTEP and memantine. It may be argued that lower receptor levels (mGLUR5) are functionally more sensitive to blockade so that drug-induced effects become stronger. However, no difference between genotypes was observed upon treatment with the mGLUR5 antagonist MTEP. Here, MTEP was administered acutely to induce a behavioural readout. This contrasts with the commonly held perception that longer-term treatment with mGLUR5 antagonists (e.g. ADX-48621; AFQ-056) may be therapeutically exploited in PD patients with levodopa-induced dyskinesia [54]. That no difference was observed for MTEP is consistent with the observations following NMDA blockade using memantine in the light/dark box. In this case, there was no effect of memantine on anxiety and locomotion in wild-type or in L62 mice, and no difference between them. While this argues for an insensitivity of the test for memantine, at least at the doses given in this study, we had hypothesised that long term administration of memantine in drinking water at doses that produced steady-state mouse plasma levels that are clinically relevant [39] might be able to reduce α-Syn induced functional changes [55]. Although we previously have reported an anxiety phenotype in L62 mice [44], this was not reproduced here possibly due to the use of mice at a younger age. Older mice did not present with a robust anxiety phenotype in the elevated plus maze [30] suggesting technical differences and age-dependent disease progression are important considerations when working with L62 mice. Overall, the abnormalities in glutamatergic receptor expression demonstrated for L62 mice did not affect the response pattern to MTEP or memantine, although the receptor changes were clearly linked to the overexpression of α-Syn. Consequently, the lowering of both NMDA and mGLUR5 receptors may be too small for induction of behavioural consequences. Consistent with a lack of post-synaptic change in glutamate functioning in L62, selective alterations of presynaptic transmitter release-mediating proteins were also not effective for induction of a hyperglutamatergic state as shown by others [56]. The use of older mice with more advanced pathology, different pharmacological tools, their combined administration, or wider dose ranges in conjunction with the application of more challenging behavioural/physiological paradigms remain to be tested to further explore these functional glutamatergic deficits.

5. Conclusions

We have demonstrated that transgenic human-α-Syn accumulates in glutamatergic synapses, and that it is able to induce a number of abnormalities in both structural and glutamate receptor proteins, both in terms of their levels and their correlations with one another. These changes were insufficient to produce corresponding differences in behavioural responses to two glutamatergic antagonists, unless these antagonists are able to override subtle functional abnormalities in synaptic function. We have confirmed that HMTM acts in the L62 mouse model of PD as an inhibitor of pathological aggregation of synuclein. We report also that HMTM treatment normalises both the ratio of NMDA receptor subunits and mGLUR5 levels. Our results therefore support the potential utility of HMTM as a disease-modifying treatment for PD aimed at decreasing synuclein aggregation pathology.

Funding

This work was funded by TauRx Therapeutics Ltd., Singapore. Z. C. was funded by the Erasmus+ programme of the European Union.

Author contributions

K. S., S. F., and G. R. conceptualised and designed the research. K. S. and Z. C. performed biochemical protein enrichment and immunoblotting, S. F. performed behavioural testing, M. M. performed immunohistology staining and manual cell counting, A. C. performed glutamate release studies, K. S prepared figures and conducted statistical analyses. K. S., and G. R wrote the manuscript and all authors contributed to the final text and approved it for publication.

Data availability

All data are provided within the manuscript or the Supporting Information.

Declaration of Competing Interest

C.R.H. and C.M.W. declare that they are officers in TauRx Therapeutics Ltd. K.S., C.R.H., C.M.W. and G.R. are named inventors on patent applications relating to HMTM and tau protein.

Acknowledgements

The authors acknowledge Dr. Dilyara Lauer and Heide Lueck for the excellent technical support with the administration of drugs, collection of brains and sectioning of brain tissue for immunohistochemistry.

Appendix A. Supplementary data

Supplementary data to this article can be found online at https://doi.org/10.1016/j.cellsig.2022.110386.

References

[1] R. Balestrino, A.H.V. Schapira, Parkinson disease, Eur. J. Neurol. 27 (2020) 27–42, https://doi.org/10.1111/ene.14108.
[2] F. Magrinelli, A. Picelli, P. Tocco, A. Federico, L. Roncari, N. Smania, G. Zanette, S. Tamburin, Pathophysiology of motor dysfunction in Parkinson's disease as the rationale for drug treatment and rehabilitation, Parkinsons. Dis. 2016 (2016), https://doi.org/10.1155/2016/9832839.
[3] E. Tolosa, Y. Compta, C. Gaig, The premotor phase of Parkinson's disease, Parkinsonism Relat. Disord. 13 (2007) 2–7, https://doi.org/10.1016/j.parkreldis.2007.06.007.
[4] C. Rodriguez-Blazquez, A. Schrag, A. Rizos, K.R. Chaudhuri, P. Martinez-Martin, D. Weintraub, Prevalence of non-motor symptoms and non-motor fluctuations in Parkinson's disease using the MDS-NMS, Mov. Disord. Clin. Pract. 8 (2021) 231–239, https://doi.org/10.1002/mdc3.13122.
[5] M. Huang, B. Wang, X. Li, C. Fu, C. Wang, X. Kang, A-Synuclein: a multifunctional player in exocytosis, endocytosis, and vesicle recycling, Front. Neurosci. 13 (2019) 1–8, https://doi.org/10.3389/fnins.2019.00028.
[6] J. Lautenschläger, C.F. Kaminski, G.S. Kaminski Schierle, α-Synuclein – regulator of exocytosis, endocytosis, or both? Trends Cell Biol. 27 (2017) 468–479, https://doi.org/10.1016/j.tcb.2017.02.002.
[7] V.M. Nemani, W. Lu, V. Berge, K. Nakamura, B. Onoa, M.K. Lee, F.A. Chaudhry, R. A. Nicoll, R.H. Edwards, Increased expression of α-synuclein reduces neurotransmitter release by inhibiting synaptic vesicle reclustering after endocytosis, Neuron. 65 (2010) 66–79, https://doi.org/10.1016/j.neuron.2009.12.023.
[8] M.J. Diógenes, R.B. Dias, D.M. Rombo, H. Vicente Miranda, F. Maiolino, P. Guerreiro, T. Näsström, H.G. Franquelim, L.M.A. Oliveira, M.A.R.B. Castanho, L. Lannfelt, J. Bergström, M. Ingelsson, A. Quintas, A.M. Sebastião, L.V. Lopes, T. F. Outeiro, Extracellular alpha-synuclein oligomers modulate synaptic transmission

and impair LTP via NMDA-receptor activation, J. Neurosci. 32 (2012) 11750–11762, https://doi.org/10.1523/JNEUROSCI.0234-12.2012.
[9] M. Baba, S. Nakajo, P.H. Tu, T. Tomita, K. Nakaya, V.M.Y. Lee, J.Q. Trojanowski, T. Iwatsubo, Aggregation of α-synuclein in Lewy bodies of sporadic Parkinson's disease and dementia with Lewy bodies, Am. J. Pathol. 152 (1998) 879–884.
[10] M.G. Spillantini, M.L. Schmidt, V.M. Lee, J.Q. Trojanowski, R. Jakes, a -Synuclein in Lewy bodies, Nature. 388 (1997) 839–840.
[11] V.M.-Y. Trojanowski, J.Q. Lee, Aggregation of neurofilament and alpha-synuclein proteins in Lewy bodies: implications for the pathogenesis of Parkinson disease and Lewy body dementia, Neurol. Rev. 55 (2) (1998) 151–152.
[12] V. Ghiglieri, V. Calabrese, P. Calabresi, Alpha-synuclein: from early synaptic dysfunction to neurodegeneration, Front. Neurol. 9 (2018), https://doi.org/10.3389/fneur.2018.00295.
[13] S. Perez-Lloret, F.J. Barrantes, Deficits in cholinergic neurotransmission and their clinical correlates in Parkinson's disease, Npj Park. Dis. 2 (2016), https://doi.org/10.1038/npjparkd.2016.1.
[14] J.C. Bridi, F. Hirth, Mechanisms of α-Synuclein induced synaptopathy in parkinson's disease, Front. Neurosci. 12 (2018) 1–18, https://doi.org/10.3389/fnins.2018.00080.
[15] B.J. Moraes, P. Coelho, L. Fão, I.L. Ferreira, A.C. Rego, Modified glutamatergic postsynapse in neurodegenerative disorders, Neuroscience. 454 (2021) 116–139, https://doi.org/10.1016/j.neuroscience.2019.12.002.
[16] G. Riedel, B. Platt, J. Micheau, Glutamate receptor function in learning and memory, Behav. Brain Res. 140 (2003) 1–47, https://doi.org/10.1016/S0166-4328(02)00272-3.
[17] N. Scheefhals, H.D. MacGillavry, Functional organization of postsynaptic glutamate receptors, Mol. Cell. Neurosci. 91 (2018) 82–94, https://doi.org/10.1016/j.mcn.2018.05.002.
[18] J. Lerma, J.M. Marques, Kainate receptors in health and disease, Neuron. 80 (2013) 292–311, https://doi.org/10.1016/j.neuron.2013.09.045.
[19] X.X. Dong, Y. Wang, Z.H. Qin, Molecular mechanisms of excitotoxicity and their relevance to pathogenesis of neurodegenerative diseases, Acta Pharmacol. Sin. 30 (2009) 379–387, https://doi.org/10.1038/aps.2009.24.
[20] N.S. Bamford, H. Zhang, Y. Schmitz, N.P. Wu, C. Cepeda, M.S. Levine, C. Schmauss, S.S. Zakharenko, L. Zablow, D. Sulzer, Heterosynaptic dopamine neurotransmission selects sets of corticostriatal terminals, Neuron. 42 (2004) 653–663, https://doi.org/10.1016/S0896-6273(04)00265-X.
[21] J. Wang, F. Wang, D. Mai, S. Qu, Molecular mechanisms of glutamate toxicity in Parkinson's disease, Front. Neurosci. 14 (2020) 1–12, https://doi.org/10.3389/fnins.2020.585584.
[22] E. Dalfó, J.L. Albasanz, M. Martín, I. Ferrer, Abnormal metabotropic glutamate receptor expression and signaling in the cerebral cortex in diffuse lewy body disease is associated with irregular α-synuclein/phospholipase C (PLCβ1) interactions, Brain Pathol. 14 (2004) 388–398, https://doi.org/10.1111/j.1750-3639.2004.tb00082.x.
[23] J.L. Albasanz, E. Dalfó, I. Ferrer, M. Martín, Impaired metabotropic glutamate receptor/phospholipase C signaling pathway in the cerebral cortex in Alzheimer's disease and dementia with Lewy bodies correlates with stage of Alzheimer's-disease-related changes, Neurobiol. Dis. 20 (2005) 685–693, https://doi.org/10.1016/j.nbd.2005.05.001.
[24] A.A. Khundakar, P.S. Hanson, D. Erskine, N.Z. Lax, J. Roscamp, E. Karyka, E. Tsefou, P. Singh, S.J. Cockell, A. Gribben, L. Ramsay, P.G. Blain, U.P. Mosimann, D.J. Lett, M. Elstner, D.M. Turnbull, C.C. Xiang, M.J. Brownstein, J.T. O'Brien, J. P. Taylor, J. Attems, A.J. Thomas, I.G. McKeith, C.M. Morris, Analysis of primary visual cortex in dementia with Lewy bodies indicates GABAergic involvement associated with recurrent complex visual hallucinations, Acta Neuropathol. Commun. 4 (2016) 1–18, https://doi.org/10.1186/s40478-016-0334-3.
[25] E. Rockenstein, M. Mallory, M. Hashimoto, D. Song, C.W. Shults, I. Lang, E. Masliah, Differential neuropathological alterations in transgenic mice expressing α-synuclein from the platelet-derived growth factor and Thy-1 promoters, J. Neurosci. Res. 68 (2002) 568–578, https://doi.org/10.1002/jnr.10231.
[26] L. Crews, H. Mizuno, P. Desplats, E. Rockenstein, A. Adame, C. Patrick, B. Winner, J. Winkler, E. Masliah, α-Synuclein alters Notch-1 expression and neurogenesis in mouse embryonic stem cells and in the hippocampus of transgenic mice, J. Neurosci. 28 (2008) 4250–4260, https://doi.org/10.1523/JNEUROSCI.0066-08.2008.
[27] E. Masliah, E. Rockenstein, I. Veinbergs, M. Mallory, M. Hashimoto, A. Takeda, Y. Sagara, A. Sisk, L. Mucke, Dopaminergic loss and inclusion body formation in α-synuclein mice: implications for neurodegenerative disorders, Science (80-). 287 (2000) 1265–1269, https://doi.org/10.1126/science.287.5456.1265.
[28] C. Rieker, K.K. Dev, K. Lehnhoff, S. Barbieri, I. Ksiazek, S. Kauffmann, S. Danner, H. Schell, C. Boden, M.A. Ruegg, P.J. Kahle, H. van der Putten, D.R. Shimshek, Neuropathology in mice expressing mouse alpha-synuclein, PLoS One 6 (2011), https://doi.org/10.1371/journal.pone.0024834.
[29] D. Amschl, J. Neddens, D. Havas, S. Flunkert, R. Rabl, H. Römer, E. Rockenstein, E. Masliah, M. Windisch, B. Hutter-Paier, Time course and progression of wild type α-Synuclein accumulation in a transgenic mouse model, BMC Neurosci. 14 (2013), https://doi.org/10.1186/1471-2202-14-6.
[30] S. Frahm, V. Melis, D. Horsley, J.E. Rickard, G. Riedel, P. Fadda, M. Scherma, C. R. Harrington, C.M. Wischik, F. Theuring, K. Schwab, Alpha-Synuclein transgenic mice, h-α-SynL62, display α-Syn aggregation and a dopaminergic phenotype reminiscent of Parkinson's disease, Behav. Brain Res. 339 (2018) 153–168, https://doi.org/10.1016/j.bbr.2017.11.025.
[31] M. König, B. Berlin, K. Schwab, S. Frahm, F. Theuring, C.M. Wischik, C. R. Harrington, G. Riedel, J. Klein, Increased cholinergic response in α-synuclein transgenic mice (h-α-synL62), ACS Chem. Neurosci. 10 (2019) 1915–1922, https://doi.org/10.1021/acschemneuro.8b00274.
[32] N.P. du Sert, V. Hurst, A. Ahluwalia, S. Alam, M.T. Avey, M. Baker, W.J. Browne, A. Clark, I.C. Cuthill, U. Dirnagl, M. Emerson, P. Garner, S.T. Holgate, D. W. Howells, N.A. Karp, S.E. Lazic, K. Lidster, C.J. MacCallum, M. Macleod, E. J. Pearl, O.H. Petersen, F. Rawle, P. Reynolds, K. Rooney, E.S. Sena, S. D. Silberberg, T. Steckler, H. Würbel, The arrive guidelines 2.0: updated guidelines for reporting animal research, PLoS Biol. 18 (2020) 1–12, https://doi.org/10.1371/journal.pbio.3000410.
[33] N.D.P. Cosford, J. Roppe, L. Tehrani, E.J. Schweiger, T.J. Seiders, A. Chaudary, S. Rao, M.A. Varney, [3H]-methoxymethyl-MTEP and [3H]-methoxy-PEPy: potent and selective radioligands for the metabotropic glutamate subtype 5 (mGlu5) receptor, Bioorg. Med. Chem. Lett. 13 (2003) 351–354, https://doi.org/10.1016/S0960-894X(02)00997-6.
[34] M.S. Cowen, E. Djouma, A.J. Lawrence, The metabotropic glutamate 5 receptor antagonist 3-[(2-methyl-1,3-thiazol- 4-yl)ethynyl]-pyridine reduces ethanol self-administration in multiple strains of alcohol-preferring rats and regulates olfactory glutamatergic systems, J. Pharmacol. Exp. Ther. 315 (2005) 590–600, https://doi.org/10.1124/jpet.105.090449.
[35] G. Yamreudeewong, W. Teixeira, G. Mayer, Stability of memantine in an extemporaneously prepared oral liquid, Int. J. Pharm. Compd. 4 (2006) 316–317.
[36] G.M. Alley, J.A. Bailey, D.M. Chen, B. Ray, L.K. Puli, H. Tanila, P.K. Banerjee, D. K. Lahiri, Memantine lowers amyloid-β peptide levels in neuronal cultures and in APP/PS1 transgenic mice, J. Neurosci. Res. 88 (2010) 143–154, https://doi.org/10.1002/jnr.22172.
[37] H. Dong, C.M. Yuede, C. Coughlan, B. Lewis, J.G. Csernansky, Effects of memantine on neuronal structure and conditioned fear in the Tg2576 mouse model of Alzheimer's disease, Neuropsychopharmacology. 33 (2008) 3226–3236, https://doi.org/10.1038/npp.2008.53.
[38] J. Lockrow, H. Boger, H. Bimonte-Nelson, A.C. Granholm, Effects of long-term memantine on memory and neuropathology in Ts65Dn mice, a model for Down syndrome, Behav. Brain Res. 221 (2011) 610–622, https://doi.org/10.1016/j.bbr.2010.03.036.
[39] R. Minkeviciene, P. Banerjee, H. Tanila, Memantine improves spatial learning in a transgenic mouse model of Alzheimer's disease, J. Pharmacol. Exp. Ther. 311 (2004) 677–682, https://doi.org/10.1124/jpet.104.071027.
[40] G. Paxinos, K. Franklin, The Mouse Brain in Stereotaxic Coordinates, Compact, 5th Editio, Academic Press, 2019.
[41] A. Saul, O. Wirths, Endogenous apolipoprotein E (ApoE) fragmentation is linked to amyloid pathology in transgenic mouse models of Alzheimer's disease, Mol. Neurobiol. 54 (2017) 319–327, https://doi.org/10.1007/s12035-015-9674-4.
[42] H. Breyhan, O. Wirths, K. Duan, A. Marcello, J. Rettig, T.A. Bayer, APP/PS1KI bigenic mice develop early synaptic deficits and hippocampus atrophy, Acta Neuropathol. 117 (2009) 677–685, https://doi.org/10.1007/s00401-009-0539-7.
[43] S. Won, S. Incontro, R.A. Nicoll, K.W. Roche, PSD-95 stabilizes NMDA receptors by inducing the degradation of STEP61, Proc. Natl. Acad. Sci. U. S. A. 113 (2016) E4736–E4744, https://doi.org/10.1073/pnas.1609702113.
[44] K. Schwab, S. Frahm, D. Horsley, J.E. Rickard, V. Melis, E.A. Goatman, M. Magbagbeolu, M. Douglas, M.G. Leith, T.C. Baddeley, J.M.D. Storey, G. Riedel, C.M. Wischik, C.R. Harrington, F. Theuring, A protein aggregation inhibitor, leuco-methylthioninium bis(Hydromethanesulfonate), decreases α-synuclein inclusions in a transgenic mouse model of synucleinopathy, Front. Mol. Neurosci. 10 (2018) 1–15, https://doi.org/10.3389/fnmol.2017.00447.
[45] P. Garcia-Reitböck, O. Anichtchik, A. Bellucci, M. Iovino, C. Ballini, E. Fineberg, B. Ghetti, L. Della Corte, P. Spano, G.K. Tofaris, M. Goedert, M.G. Spillantini, SNARE protein redistribution and synaptic failure in a transgenic mouse model of Parkinson's disease, Brain. 133 (2010) 2032–2044, https://doi.org/10.1093/brain/awq132.
[46] C. Agliardi, M. Meloni, F.R. Guerini, M. Zanzottera, E. Bolognesi, F. Baglio, M. Clerici, Oligomeric α-Syn and SNARE complex proteins in peripheral extracellular vesicles of neural origin are biomarkers for Parkinson's disease, Neurobiol. Dis. 148 (2021), 105185, https://doi.org/10.1016/j.nbd.2020.105185.
[47] A. Lleó, R. Núñez-Llaves, D. Alcolea, C. Chiva, D. Balateu-Paños, M. Colom-Cadena, G. Gomez-Giro, L. Muñoz, M. Querol-Vilaseca, J. Pegueroles, L. Rami, A. Lladó, J. L. Molinuevo, M. Tainta, J. Clarimón, T. Spires-Jones, R. Blesa, J. Fortea, P. Martínez-Lage, R. Sánchez-Valle, E. Sabidó, À. Bayés, O. Belbin, Changes in synaptic proteins precede neurodegeneration markers in preclinical Alzheimer's disease cerebrospinal fluid*, Mol. Cell. Proteomics 18 (2019) 546–560, https://doi.org/10.1074/mcp.RA118.001290.
[48] E.B. Mukaetova-Ladinska, F. Garcia-Siera, J. Hurt, H.J. Gertz, J.H. Xuereb, R. Hills, C. Brayne, F.A. Huppert, E.S. Paykel, M. McGee, R. Jakes, W.G. Honer, C. R. Harrington, C.M. Wischik, Staging of cytoskeletal and β-amyloid changes in human isocortex reveals biphasic synaptic protein response during progression of Alzheimer's disease, Am. J. Pathol. 157 (2000) 623–636, https://doi.org/10.1016/S0002-9440(10)64573-7.
[49] Z. Zhang, S. Zhang, P. Fu, Z. Zhang, K. Lin, J.K.S. Ko, K.K.L. Yung, Roles of glutamate receptors in Parkinson's disease, Int. J. Mol. Sci. 20 (2019) 1–17, https://doi.org/10.3390/ijms20184391.
[50] K. Lepeta, M.V. Lourenco, B.C. Schweitzer, P.V. Martino Adami, P. Banerjee, S. Catuara-Solarz, M. de La Fuente Revenga, A.M. Guillem, M. Haidar, O. M. Ijomone, B. Nadorp, L. Qi, N.D. Perera, L.K. Refsgaard, K.M. Reid, M. Sabbar, A. Sahoo, N. Schaefer, R.K. Sheean, A. Suska, R. Verma, C. Vicidomini, D. Wright, X.D. Zhang, C. Seidenbecher, Synaptopathies: synaptic dysfunction in neurological disorders – a review from students to students, J. Neurochem. (2016) 785–805, https://doi.org/10.1111/jnc.13713.

[51] H. Mizuno, M.S. Rao, H. Mizuno, T. Sato, S. Nakazawa, T. Iwasato, NMDA receptor enhances correlation of spontaneous activity in neonatal barrel cortex, J. Neurosci. 41 (2021) 1207–1217, https://doi.org/10.1523/JNEUROSCI.0527-20.2020.

[52] X.P. Wang, P. Ye, J. Lv, L. Zhou, Z.Y. Qian, Y.J. Huang, Z.H. Mu, X. Wang, X. Jie Liu, Q. Wan, Z.H. Yang, F. Wang, Y.Y. Zou, Expression changes of NMDA and AMPA receptor subunits in the hippocampus in rats with diabetes induced by Streptozotocin coupled with memory impairment, Neurochem. Res. 44 (2019) 978–993, https://doi.org/10.1007/s11064-019-02733-4.

[53] S.R. Das, R. Jensen, R. Kelsay, M. Shumaker, R. Bochart, B. Brim, D. Zamzow, K. R. Magnusson, Reducing expression of GluN1 0XX subunit splice variants of the NMDA receptor interferes with spatial reference memory, Behav. Brain Res. 230 (2012) 317–324, https://doi.org/10.1016/j.bbr.2012.02.014.

[54] C. Lu Zhang, Q. Wen Han, N. Hong Chen, Y. He Yuan, Research on developing drugs for Parkinson's disease, Brain Res. Bull. 168 (2021) 100–109, https://doi.org/10.1016/j.brainresbull.2020.12.017.

[55] J.E. Lee, H.N. Kim, D.Y. Kim, Y.J. Shin, J.Y. Shin, P.H. Lee, Memantine exerts neuroprotective effects by modulating α-synuclein transmission in a parkinsonian model, Exp. Neurol. 344 (2021), 113810, https://doi.org/10.1016/j.expneurol.2021.113810.

[56] M. Emre, M. Tsolaki, U. Bonuccelli, A. Destée, E. Tolosa, A. Kutzelnigg, A. Ceballos-Baumann, S. Zdravkovic, A. Bladström, R. Jones, Memantine for patients with Parkinson's disease dementia or dementia with Lewy bodies: a randomised, double-blind, placebo-controlled trial, Lancet Neurol. 9 (2010) 969–977, https://doi.org/10.1016/S1474-4422(10)70194-0.